



Petrophysical and acoustic assessment of carbonate rocks, Zahle area, central Lebanon

Mohamed K. Salah¹ · Mohammad Alqudah² · Christian David³

Received: 5 July 2019 / Accepted: 25 June 2020 / Published online: 7 July 2020
© Springer-Verlag GmbH Germany, part of Springer Nature 2020

Abstract

Transport and acoustic measurements have been conducted on fifteen rock samples collected from central Lebanon to characterize the rock properties and to assess the impact of lithology, pore types, pore sizes, and textural parameters on the storage capacity and elastic characteristics. The spontaneous imbibition of selected samples was examined by detecting the moving capillary front across a sample. The coefficient of capillarity derived from the spontaneous imbibition is positively correlated with permeability. Seismic velocities in the studied rocks vary widely and are positively correlated with the rock density. Matrix-supported rocks with a larger proportion of micropores have lower seismic wave velocities, whereas the grain-supported carbonates exhibit low to moderate porosity and higher acoustic velocities. The elastic properties of the studied carbonates indicate a granular, rather than a crystalline, texture for the majority of the studied rocks. The widely variable elastic behavior of basically carbonate rocks implies that seismic reflection profiles in carbonate sequences may contain seismic reflections that do not result from non-carbonate intercalations but which result mainly from variable porosity, pore types, and shapes in the carbonate rocks themselves. This study provides important information on the textural, petrophysical, and elastic properties of carbonate rocks which are crucial for the assessment and understanding of the seismic reflection sections in subsurface carbonate reservoirs.

Keywords Zahle area · Central Lebanon · Transport properties, elastic properties · Shallow marine carbonates

Introduction

Carbonate rocks are important reservoirs hosting 50–60% of the hydrocarbon reserves around the world (e.g., Burchette 2012). They are characterized by complex fabric and pore geometry which together represent major challenges in the interpretation of seismic data and fluid transport properties. A comprehensive understanding of the relationships between carbonate rock fabric, their porosity and acoustic velocity is essential for interpreting seismic sections and borehole acoustic logs (e.g., Verwer et al.

2008; Regnet et al. 2015; Soete et al. 2015). Assessment of the impact of the storage capacity properties such as porosity, permeability, and rock density on acoustic velocity helps to analyze the origin of reflections on seismic sections and to calculate the impedance models to compute seismic synthetic sections (Biddle et al. 1992; Campbell and Stafleu 1992; Verwer et al. 2008). The nature of the interface between wetting and non-wetting fluids (e.g., water and oil, respectively), which is valuable for hydrocarbon recovery, is a very complex task in carbonate strata and is controlled by the rock microstructures (David et al. 2008, 2011; Pons et al. 2011). The obtained information on the pore microstructures is quantitatively valuable for the modeling of fluid flow processes in porous geomaterials (David et al. 2015).

Many factors control the acoustic properties of carbonate rocks such as pore shape and type, total porosity, pore fluid nature, and rock fabric, making it extremely difficult to attribute the observed variations in the measured seismic velocity to any of these controlling parameters (Wang et al. 1991; Anselmetti and Eberli 1993, 1999; Anselmetti et al. 1997; Kenter et al. 1997, 2002, 2007; Dürrast and Siegesmund 1999; Brigaud et al. 2010; Casteleyn et al. 2010, 2011;

✉ Mohamed K. Salah
ms264@aub.edu.lb

¹ Department of Geology, American University of Beirut, Riad El Solh, Beirut 1107 2020, Lebanon

² Earth and Environment Sci. Department., Faculty of Science, Yarmouk University, Irbid 21163, Jordan

³ Department of Geosciences & Environment, CY Cergy Paris Université, F-95031 Cergy-Pontoise, France

Regnet et al. 2015). Moreover, carbonate rocks have, by virtue of their nature, very high diagenetic potential which can easily alter basic rock parameters such as crystal morphology, porosity, and rock rigidity (Braaksma et al. 2003; Verwer et al. 2008). The major diagenetic processes affecting carbonate rocks are compaction, dissolution, cementation, recrystallization, and dolomitization, which may enhance or diminish the rock porosity and, in extreme cases, can totally alter the rock mineralogy and pore fabric (Eberli et al. 2003; Salah et al. 2016). In addition, cementation of micrite and the subsequent changes in fluid saturation have strong impacts on the response of both electrical resistivity and sonic borehole logging in carbonate reservoirs (Fabricius 2003; Fabricius et al. 2007).

Many limestones have different velocities at a given porosity (Sun et al. 2006), and even different porosities at a certain velocity, which are difficult to predict from published models of the porosity-velocity (φ - V) or velocity/density correlations. Therefore, unlike clastic reservoir rocks, theories which describe the propagation of seismic waves in porous media (Gassmann 1951; Biot 1956a, 1956b) are inapplicable to carbonate rocks because of their complex pore network and unique diagenetic texture with unpredictable seismic properties. Simple theories and relationships, as those of Wyllie et al. (1956, 1958), and Raymer et al. (1980), which describe the propagation of seismic wave velocities in sandstones are difficult to apply for pure limestones (Brigaud et al. 2010). Most of the previous studies on the φ - V relationship have been focusing on grain-supported carbonate rocks having a higher proportion of macropores and thus more permeable and much more significant fluid flow and hydrocarbon recovery. In the giant oil fields of the Middle East, microporous carbonate reservoirs are common and represent a significant component of reservoir rocks in the region (Nurmi and Standen 1997; Ehrenberg et al. 2008). These rocks were not adequately studied because, compared with granular limestones, they are less permeable, ineffectively contributing to fluid flow, and hinder the extraction of their hydrocarbon content (Ehrenberg et al. 2008; Vanorio and Mavko 2011). These rocks, although porous with sometimes porosities between 8 and 30%, are characterized generally by low (rarely moderate) permeability (Kaldi 1989; Moshier 1989; Deville de Periere et al. 2011). The intercrystalline micropores in these carbonate rocks occur usually in a lithified matrix of microcrystalline calcite which is known as micritie (Folk 1966).

In addition to the value of limestones as common reservoir rocks all over the world, the carbonate rocks of Lebanon are good karst aquifers and are highly significant engineering and construction materials (e.g., Nader and Swennen 2004). In this study, we are concerned with the analysis of fifteen rock samples collected from the Paleogene strata exposed in Zahle, central Lebanon to investigate their petrography, nannofossil content, as well as other thin-section-derived parameters. In addition, we measure the basic fluid transport and elastic properties

including porosity, permeability, density, electrical conductivity, capillarity, and the acoustic wave velocities and then interpret the observed measurements utilizing the results of the petrographic and scanning electron microscope (SEM) investigations. The study of the spontaneous imbibition of selected porous samples provides valuable information on the fluid flow across reservoir rocks. The present study provides also important clues on the factors affecting the propagation of elastic waves and the physical characteristics of microporous limestones, hence upgrading our current understanding on the interconnections between the petrophysical and acoustic properties as well as the microstructural features of carbonate rocks.

Geologic setting and stratigraphy

During the Paleogene, the Arabian Plate was located between the Tropic of Cancer and the Equator (Beydoun 1991; Alsharhan and Nairn 1995; Sharland et al. 2001). During this time, the opening of both the Atlantic and the Indian Oceans has resumed, resulting in a continuous northward movement of Arabia toward Eurasia and rapidly closing the Neo-Tethys Ocean, an event that inherited a deep foreland basin near the plate margin (Sharland et al. 2001). Thus, the early Paleogene times of Lebanon are dominated by deep carbonate platform of a monotonous chalky, fine-grained character, which is partially rich in organic matter.

The lower and middle Eocene rocks in central Lebanon overlie the thick chalky Paleocene successions and are represented mainly by two facies: one is a chalky limestone, often with chert concretions which is common in basin deposits, while the other is a nummulitic limestone which is found on the basin margins. The chalky limestone facies is geographically limited due to the influence of the Syrian Arc event on the region (Alqudah et al. 2019). This rock sequence has a total thickness of 400 m in Zahle (Fig. 1) where it is well-exposed (Walley 1997). The encountered facies reflect clearly the influence of tectonics on the area during the Paleogene (Walley 1997; Alqudah et al. 2019).

Tectonic events, mainly the collision between Arabia and Eurasia, affected the sedimentation pattern in the region causing a regional uplift, which resulted in the formation of the paleolake of Zahle (Beydoun 1999; Sharland et al. 2001). Neogene rocks of the Bekaa valley include deposits of non-marine origin containing non-marine microfossils such as charophytes, gastropods, and ostracods (Sanjuan and Alqudah 2018). The preservation and diversity of these microfossils imply that the paleolake of Zahle was well-established and characterized by a permanent, shallow oligotrophic freshwater.

Materials and methods

The studied samples were collected from two closely spaced exposures in Zahle, the first of which is the early and middle

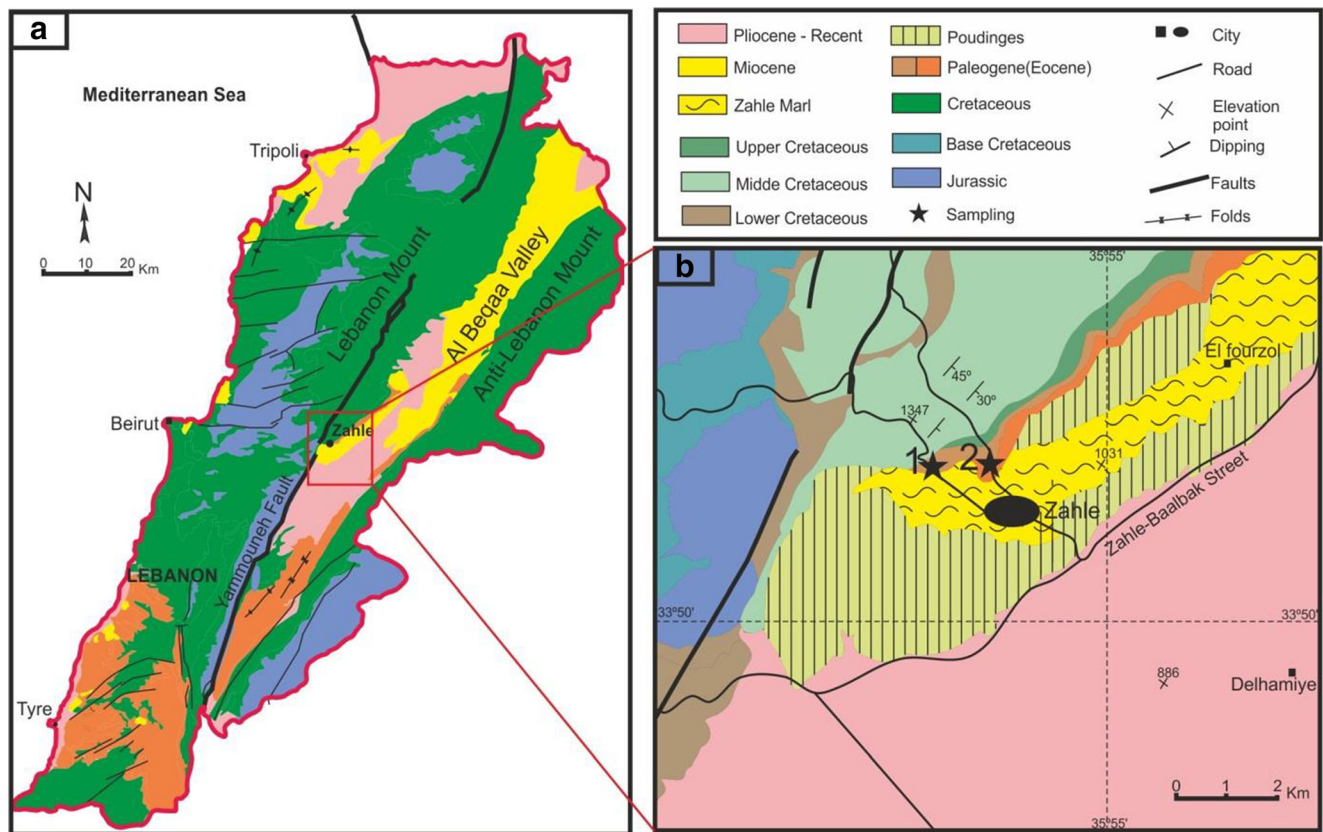


Fig. 1 Geological map of Lebanon in the Eastern Mediterranean region (a), with an inset (b) representing the details of the studied rock exposures in Zahle area which are shown by the red rectangle in (a)

Eocene sequence where the chalky limestones enriched in planktonic foraminifera and calcareous nannofossils (Fig. 2 and Fig. 3a–c) prograde to the middle Eocene shallow marine platform rocks which are represented by a *nummulitic* bank (Fig. 3d). The second location is about 1 km away from the first one, the sediments of which belong mainly to the Miocene (Fig. 1). The exposed rocks in this location are composed essentially of mixtures of marl to marly limestones with some intercalations of ash and lignites (Fig. 3 e and f).

Fifteen rock samples were collected from the Paleogene and Neogene deposits in Zahle. The number of samples that were obtained from the chalky limestones, the nummulitic limestones, and from the Neogene deposits are ten, two, and three, respectively. Core samples were extracted from fresh outcrops using a portable, gasoline-powered, core-driller (Model D261-C). Thin sections were prepared from all collected samples and then examined under the polarized microscope to identify the standard microfacies, to differentiate between the primary and secondary porosity, to investigate the different post-depositional diagenetic processes, and to relate these features to the prevailing paleoenvironmental conditions. The procedures described in Salah et al. (2018), and references therein, were followed here to characterize porosity, its origin, grain types, cement and matrix nature, sorting, and

any observed diagenetic process. We also examined the calcareous nannofossil content of the rock samples, which provides additional constraints on the paleoecology. The obtained results are listed in Table 1.

Field-drilled plugs were subsequently slivered in the lab to optimum lengths of 2–5-cm long, cleaned with distilled water, and then dried at a temperature of 80 °C for 24 h (Mavko et al. 2009). Porosity (φ) was determined by the triple weight method using water as the saturating liquid. This method gives the effective porosity of a rock sample since it is only the connected pore spaces that are occupied by the saturating fluid.

The bulk density (ρ_b , g/cm³) is calculated from the dry mass of the core sample divided by its bulk volume obtained during the porosity measurement, whereas the grain density (ρ_g , g/cm³) is calculated from the porosity and bulk density using the relation: $\rho_g = \rho_b / (1 - \varphi)$.

Permeability is measured by applying Darcy’s law using nitrogen gas and converted automatically to the liquid permeability (K_L) as proposed by Klinkenberg (1941). The electrical conductivity was measured twice, first after samples were saturated with tap water (water conductivity; $\sigma_w = 0.66$ mS/m) and then with saline water ($\sigma_w = 58$ mS/m). The formation resistivity factor (F), at the two different brine concentrations, was calculated from the electrical conductivity of the rock

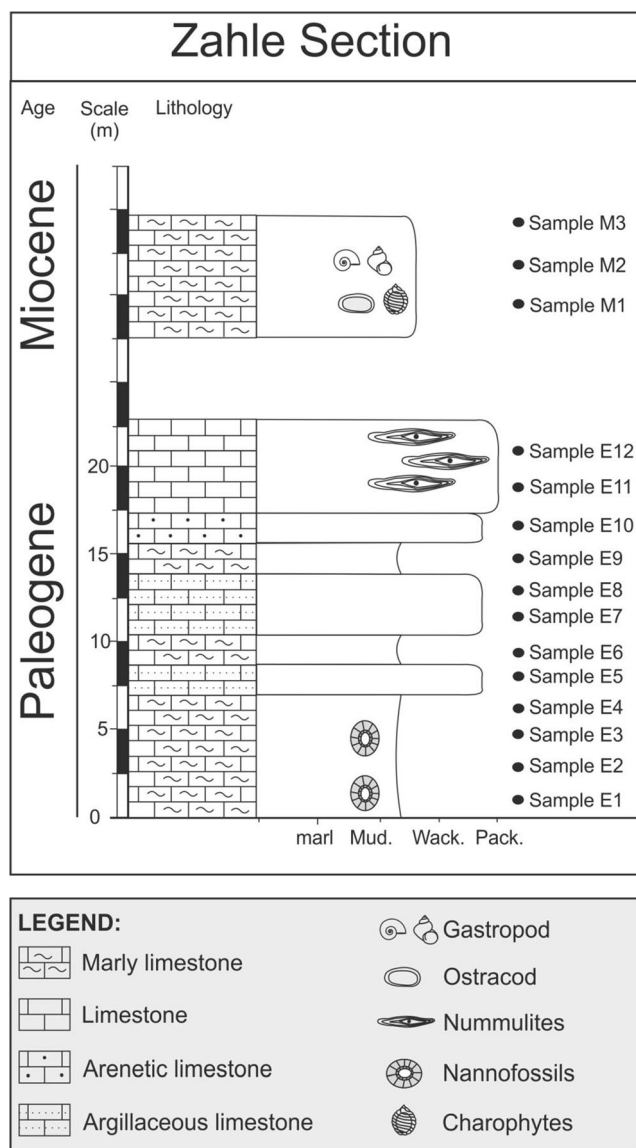


Fig. 2 Columnar section of the Paleogene succession exposed in Zahle area

sample (σ_r) and the water conductivity as $F = \sigma_w / \sigma_r$. The obtained petrophysical and electrical conductivity data are listed in Table 2.

Many methods are available to study the capillary imbibition and to monitor the moving capillary front in rocks such as the standard weight increase measurement, X-ray imaging, and ultrasonic monitoring (David et al. 2015). In this study, we used the routine mass increase method due to the water intake with time to determine the coefficient of capillarity and examine its relationship with permeability and the rock microtexture. This was accomplished through continuously weighing a sample while monitoring the height of the water front during imbibition (Siebold et al. 1997). The resulting data are presented by plotting the water absorption as a function of the radical of time. In this way, a straight line would be

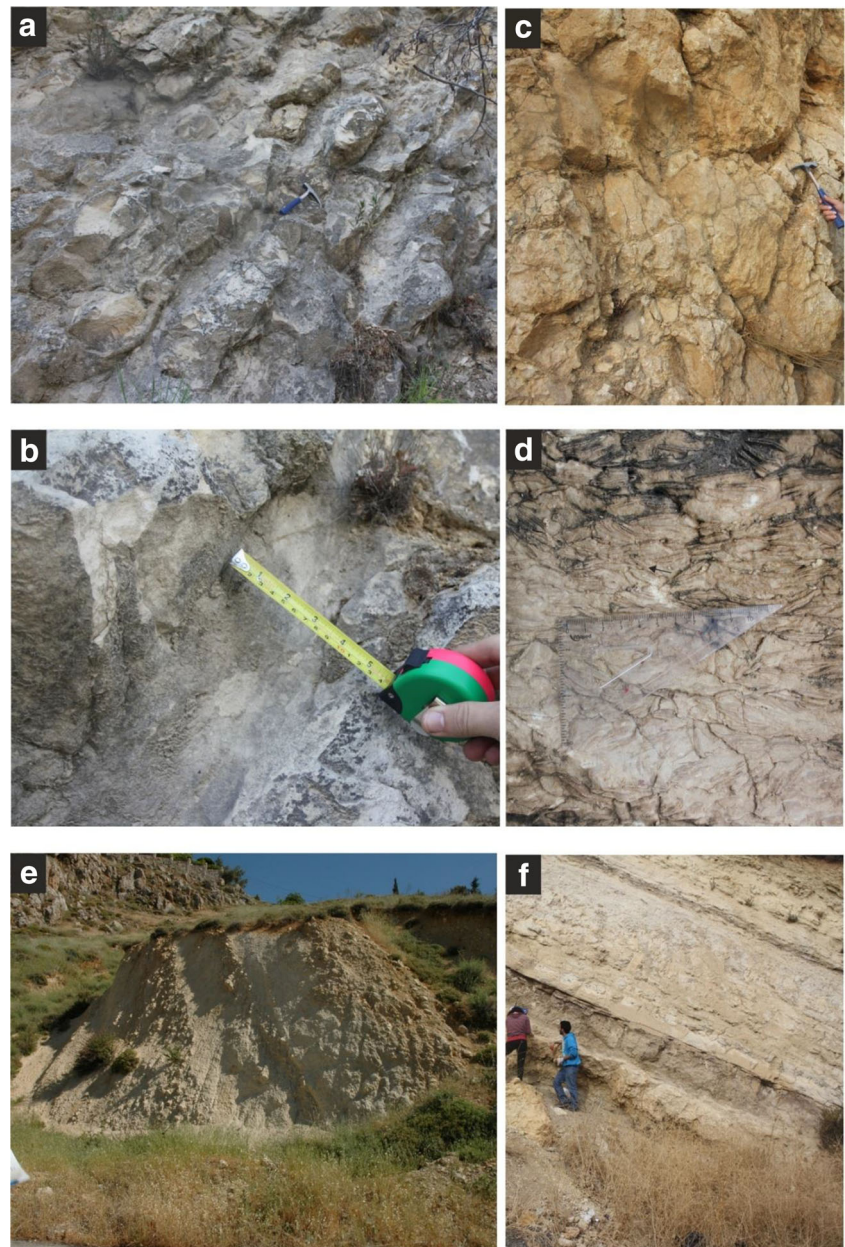
obtained if the porous rock is replaced by one pipe of constant radius r . Because Earth materials are often inhomogeneous, this linear relationship is never discerned for normal rocks. However, the capillarity (C) parameter can be estimated from the average slope of the plot between the mass of water versus the square root of time plot: $C = 1/\pi R^2 \cdot dm/d(t)^{0.5}$, with R being the sample radius, m is the water mass intake, and t is time.

Primary and secondary wave velocities (V_p , and V_s) were first measured for the dried plugs at ambient conditions using Panametrics Pulser-Receiver (Model 5058PR) and an Agilent DSO-X-2014A Digital Storage Oscilloscope (100 MHz). Two transducers are attached firmly to the plug ends, and the travel time of the acoustic pulse across the core is read on a screen with an accuracy of $0.01 \mu\text{s}$ and then used, along with the core length, to calculate the corresponding seismic velocity. Three measurements of velocity at perpendicular directions have been taken for each core, and the results averaged in order to account for any possible anisotropy and to have a more representative velocity for each rock sample (e.g., Soete et al. 2015). Acoustic velocities are strongly affected by fluids due to scattering, rock-fluid interaction, and local grain-scale flow effects (Mavko and Jizba 1991). Fluid saturation causes also velocity dispersion where the measured velocity increases with the measurement frequency, whereas the seismic velocity in dry rocks is insensitive to the frequency (Mavko et al. 1998; Khazanehdari and Sothcott 2003). Therefore, both V_p and V_s have been re-measured for the water-saturated samples. The obtained bulk density and acoustic wave velocities were used to compute the acoustic impedance and the Poisson's (ν) ratio of the studied rocks. The ν ratio is the ratio between transverse contractions over longitudinal stretching of a stressed sample and controls the speed and reflection of seismic waves and, therefore, is substantial for anticipating the quality of rocks (e.g., Rafavich et al. 1984; Soete et al. 2015). It is calculated from V_p and V_s as follows (e.g., Mavko et al. 1998):

$$\nu = (V_p^2 - 2V_s^2) / 2(V_p^2 - V_s^2).$$

In seismology, the ν ratio is used as an indicator of the physical properties and the fluid content in rocks, as well as the seismogenic behavior of the Earth's crust (Zhao et al. 1996; Zhao and Negishi 1998; Kearey et al. 2002; Salah and Zhao 2003; Salah et al. 2011). The elastic moduli and the ν ratio relate stresses applied to rocks to resulting strains and, hence, are good measures of the rock stiffness and mechanical properties (Siegesmund and Dürrast 2014; Yu et al. 2016). The ν ratio and Young's modulus, in particular, are used to assess the mechanical behavior of rocks used in construction purposes (Gerçek 2007; Hudson et al. 2011). The combinations of either the shear and bulk moduli or the ν ratio and the Young's modulus are enough to fully characterize the mechanical properties of Earth's materials. The measured and calculated petrophysical and elastic parameters are listed in Table 2.

Fig. 3 Field photographs representing the exposed strata in the studied area: **a**, **b**, and **c** belong to the early Eocene rocks; **d** represents middle Eocene outcrops, whereas **e** and **f** represent the Neogene Zahle Paleolake deposits



Results and discussion

Petrography

Based on the petrography of the collected rocks, the Eocene limestones of Zahle area can be divided into two facies, fine-grained limestones (samples E1–E10) varying from wack- to packstones and coarse-grained limestones (samples E11 and E12). The collected Miocene rocks (samples M1–M3) are mainly packstones with minor wackstone intercalations (Table 1; Fig. 2).

Wackstone

Samples E1, E9, and E10 are dominantly matrix-supported with about 10% bioclasts of planktonic and benthic foraminifera which are generally well-preserved (Fig. 4 a and b; Fig. 5 d–i), in addition to some shark bone remains (Fig. 5g–h). Non-bioclasts in these samples are composed mainly of calcite; matrix is almost calcitic although it contains some amount of iron oxides. Calcium carbonate sparite either partially or completely fills the intragranular pores (Fig. 4 a and b). In the same time, secondary calcium carbonate precipitations fill the spaces in the fractures (Fig. 4c).

Table 1 Summary of the main results of the petrographic investigation of the studied rocks

Sample No	Rock name	Grain ratio		Porosity	Matrix	Cement	Crystal shapes	Grain size and packing
		Bioclast	Non-bioclast					
E1	Wackstone	10% planktic and benthic foraminifera	Rare, calcite	Fractures filled by secondary calcium carbonate	80% calcitic	Rare calcitic sparite	Small grains	Matrix supported
E2–E3	Packstone	20% planktic, benthic foraminifera, and bones fragments	20% calcite	Fenestral pores resulted from cementation	Iron oxide and calcite	Microsparite is available	Well-sorted crystals	Grain supported
E4	Wackstone-packstone	10% well and poor-preserved foraminifera	10% calcitic	Intragranular resulted from broken forams	70% calcite and iron oxide	Rare calcitic fill inside forams	Irregular crystal shapes	Matrix supported
E5–E6	Wackstone-packstone	10% planktic and benthic forams	5% calcite crystals	Intragranular intergranular, vuggy resulted from dissolution	Calcitic micrite	Partial fill in the pores	Irregular crystal shapes	Matrix supported
E7	Wackstone-packstone	20% planktic and benthic foraminifera	10% calcite lithoclast	Very low partially intragranular fenestral	70% calcite micrite	Rare calcitic fill inside forams	Matrix supported	Grain supported
E8	Packstone	30% planktic, benthic foraminifera, and gastropods	20% microcalcite crystal	Very high intragranular and fenestral	Calcite micrite is rare	Rare geodes structure, calcitic sparite	Microcrystals	Grain supported
E9	Wackstone	10% preserved planktic and benthic foraminifera	5% calcite. Rare	Intragranular, vuggy pores	85% calcite micrite	—	—	Matrix supported
E10	Wackstone	10% preserved planktic foraminifera and shark bones	5% calcite. Rare	Very low intragranular	85% calcite Micrite	—	—	Matrix supported
E11–E12	Packstone	70% benthic foraminifera	20% microcalcite crystal	Very high Intragranular and fenestral intergranular	Calcite micrite is rare	Geodes structure, calcitic sparite	Microcrystals	Grain supported
M1–M3	Packstone	60% gastropods ostracods and chrophytes	20% microcalcite crystal	Very high intragranular and intergranular	20% calcitic micrite	Geodes structure, calcitic sparite in M1 and 3	Microcrystals	Grain supported

Table 2 Petrophysical and elastic properties measured for the dry and water-saturated samples

S. No	φ	ρ_b	ρ_g	K mD	F_1	F_2	Vp	Vs	ν	E	k	G	Vp sat	Vs sat	ν sat	E sat	k sat	μ sat
E1	0.31	1.87	2.70	0.242	5.19	14.42	2979	1852	0.19	1.52	0.80	0.64	2880	1331	0.36	0.90	1.11	0.33
E2	0.16	2.27	2.70	0.020	4.48	49.07	3903	2406	0.19	3.13	1.70	1.31	3681	1910	0.32	2.17	1.97	0.83
E3	0.29	1.90	2.68	0.331	1.39	13.10	3057	1916	0.18	1.64	0.85	0.70	2477	1290	0.31	0.83	0.74	0.32
E4	0.35	1.76	2.71	1.072	4.32	15.28	3093	1890	0.20	1.51	0.85	0.63	2783	1288	0.36	0.80	0.97	0.29
E5	0.12	2.40	2.72	0.205	35.56	59.96	5209	2634	0.33	4.42	4.29	1.66	4963	2548	0.32	4.11	3.83	1.56
E6	0.34	1.78	2.69	0.774	4.92	11.93	2780	1732	0.18	1.26	0.66	0.53	2518	1118	0.38	0.61	0.83	0.22
E7	0.30	1.88	2.70	0.758	4.61	14.85	3055	1884	0.19	1.59	0.87	0.67	2789	1369	0.34	0.95	1.99	0.35
E8	0.24	2.05	2.70	0.171	6.29	24.46	3368	2023	0.22	2.05	1.21	0.84	3231	1532	0.35	1.31	0.50	0.48
E9	0.39	1.63	2.68	0.576	2.40	9.70	2531	1613	0.16	0.98	0.48	0.42	2070	805	0.41	0.30	0.56	0.11
E10	0.32	1.80	2.66	0.293	1.90	11.64	2828	1810	0.15	1.36	0.65	0.59	2378	967	0.40	0.47	0.79	0.17
E11	0.01	2.68	2.70	0.005	703.11	5599.23	6449	3292	0.32	7.68	7.26	2.90	6406	3062	0.35	6.78	7.63	2.51
E12	0.01	2.67	2.70	0.007	1154.14	3651.55	6329	3228	0.32	7.36	6.98	2.78	6482	3202	0.34	7.32	7.56	2.74
M1	0.17	2.22	2.67	0.572	34.92	158.66	4654	2565	0.28	3.74	2.86	1.46	5031	2388	0.35	3.43	3.93	1.26
M2	0.40	1.62	2.72	9.013	3.69	7.21	2281	1438	0.17	0.79	0.40	0.34	2441	1439	0.23	0.83	0.52	0.34
M3	0.05	2.49	2.62	0.007	306.74	5961.84	5651	2915	0.32	5.58	5.13	2.12	5720	2761	0.35	5.12	5.61	1.90
Min	0.01	1.62	2.62	0.005	1.39	7.21	2281	1438	0.15	0.79	0.40	0.34	2070	805	0.23	0.30	0.52	0.11
Max	0.40	2.68	2.72	9.013	1154.14	5961.84	6449	3292	0.33	7.68	7.26	2.90	6482	3202	0.41	7.32	7.63	2.74
Avg	0.23	2.07	2.69	0.936	151.58	1040.19	3878	2213	0.23	2.97	2.33	1.17	3723	1801	0.35	2.40	2.57	0.89

φ , porosity (fraction); ρ_b and ρ_g , bulk and grain densities (g/cm^3); K , permeability in millidarcys; F_1 and F_2 , the formation resistivity factors at two measurement cycles; Vp and Vs, the primary and secondary wave velocities (m/s); ν , Poisson's ratio; E , Young's modulus; k , bulk modulus; μ , rigidity modulus. Symbols with the suffix "sat" denote the elastic properties of the water-saturated samples. All the elastic moduli are given in 10^{10} Pa. Min, Max, and Avg are the minimum, maximum, and average value of a given parameter, respectively

Wack-/packstone

This microfacies is detected in samples E4–E7 where the percentage of bioclasts increased slightly. Both well- and poorly-preserved planktonic and benthic foraminifera are detected, reflecting shallower marine settings during the deposition of these rocks (Fig. 4l, m, n, p, q, r, and s). Non-bioclasts are represented mainly by calcium carbonate crystals of irregular shapes. All bioclasts and non-bioclasts are floating in a ground-mass of micrite composed mainly of calcium carbonate as well as other components like iron oxides (Fig. 4l and m).

Porosity resulting from the intraparticle pores inside the foraminifera is rare in this case since they have been filled with sparite (Fig. 4l). Intergranular pores are also recognized (Fig. 4m). Although the secondary precipitation of sparite diminished the primary porosity in some cases, the pore space volume has increased in others due to the high dissolution of calcium carbonate producing sometimes very large pores (Fig. 4o). Therefore, porosity varies from moderate to high according to the degree of dissolution.

Packstone

This microfacies was detected in the majority of samples and can be divided into three, slightly different, subfacies: the first

includes samples E2, E3, and E8; the second comprises samples E11 and E12; whereas the third one includes samples M1, M2, and M3.

Samples of the first subfacies contain both bio- and non-bioclasts with a good percentage of matrix and micro-sparite in their texture. Bioclasts contain benthic and planktic foraminifera, gastropods, and bone fragments (Fig. 4d–k and Fig. 5a–c). Non-bioclasts are represented by well-sorted microcalcium carbonate crystals (Fig. 5a–c). These microcrystals resulted probably from secondary dissolution and reprecipitation of calcium carbonate as sparite crystals. Porosity is represented by intragranular spaces (Fig. 5c), with clear dissolution effects in the samples (Fig. 5a and b). The SEM imaging helped to check some processes that might have affected porosity. In this regard, two features have been observed which comprise the free formation of calcium carbonate crystals inside the foraminifera chambers as a secondary precipitation (Fig. 6-1) and the development of fenestral porosity (Fig. 6-5). These two processes have contrasting effects on porosity; the first diminishes porosity, while the second would enhance it.

The second subfacies is found in samples E11 and E12, in which the *Nummulites* sp. is the major bioclastic component. The *Nummulites* mark the margin between the continent and ocean setting pointing to a very shallow marine deposition. In

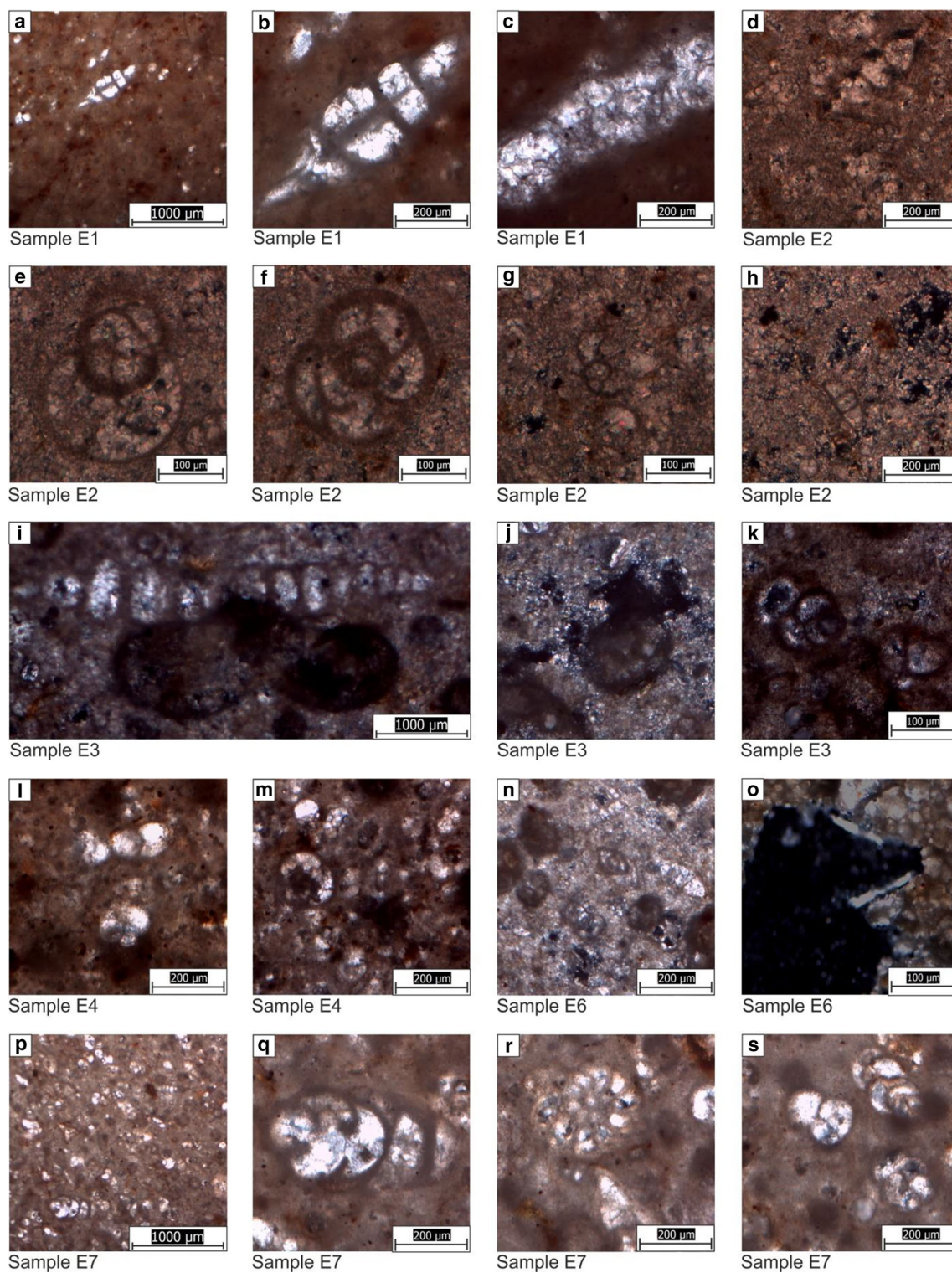


Fig. 4 A plate showing the different types of microfacies encountered in the studied samples of the early Eocene

such setting, the bioclasts, i.e., *Nummulites* sp., are dominant, while micrite is barely found (Fig. 5 k, l, and m). Porosity is very high and is represented by intergranular primary pores and fenestral secondary pores which are

filled partially with cementation followed by later dissolution (Fig. 5 j and l).

The third type of packstone subfacies is detected in the Miocene lacustrine sediments, specifically in samples M1,

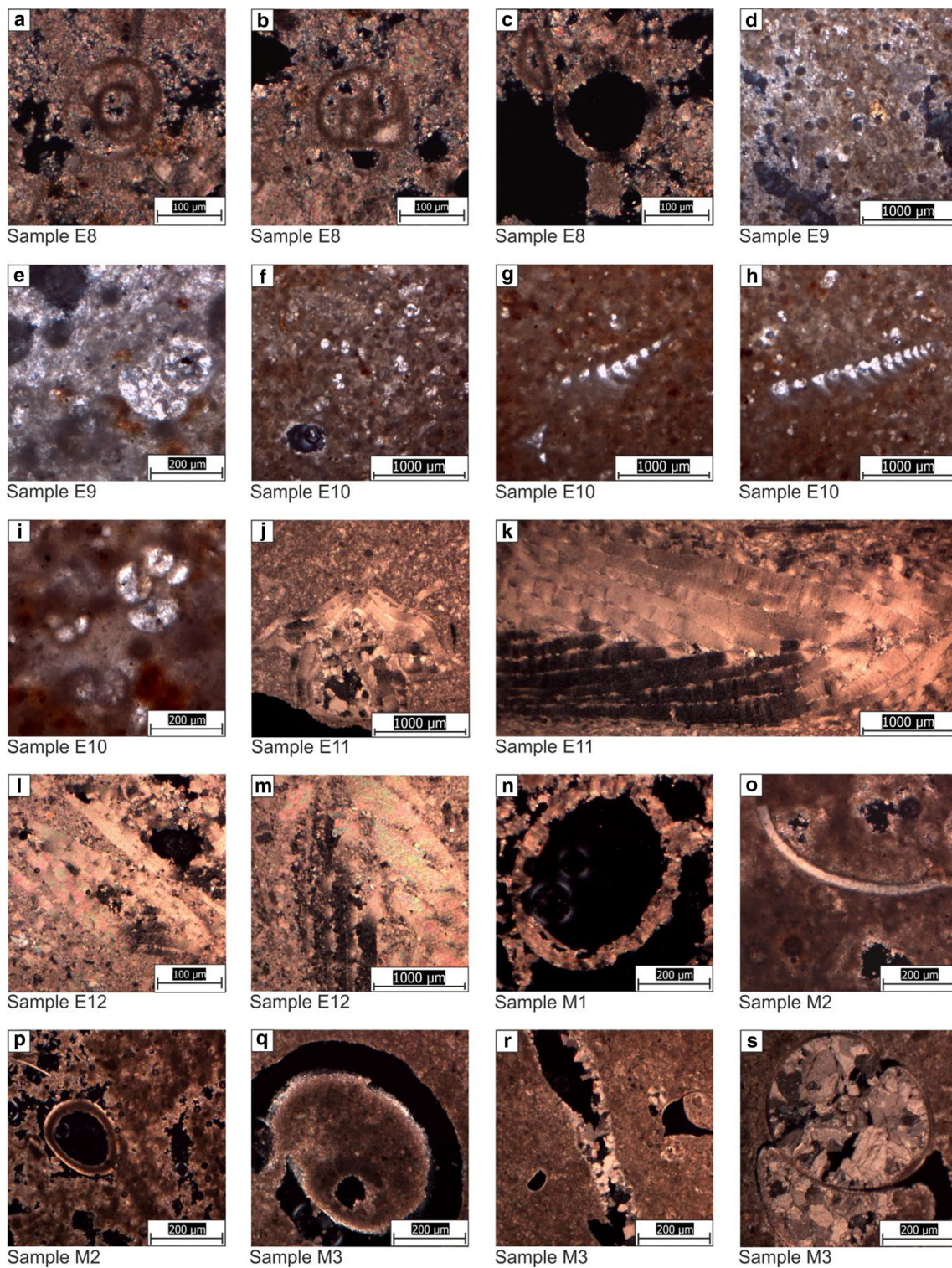


Fig. 5 A plate showing the different types of microfacies encountered in the studied samples of the late Eocene and early Miocene

M2, and M3, where a significant amount of gastropods and ostracods is encountered (Fig. 5 n and o). These bioclasts are surrounded by fine lime particles partially filling the interior of the bioclasts (Fig. 5 p and q). The sediments are barely

affected by cementation and other diagenetic processes where most of the bioclasts are not filled with precipitates of calcium carbonate although some of the grains suffered dissolution (Fig. 5q). Some samples, however, show an evidence of

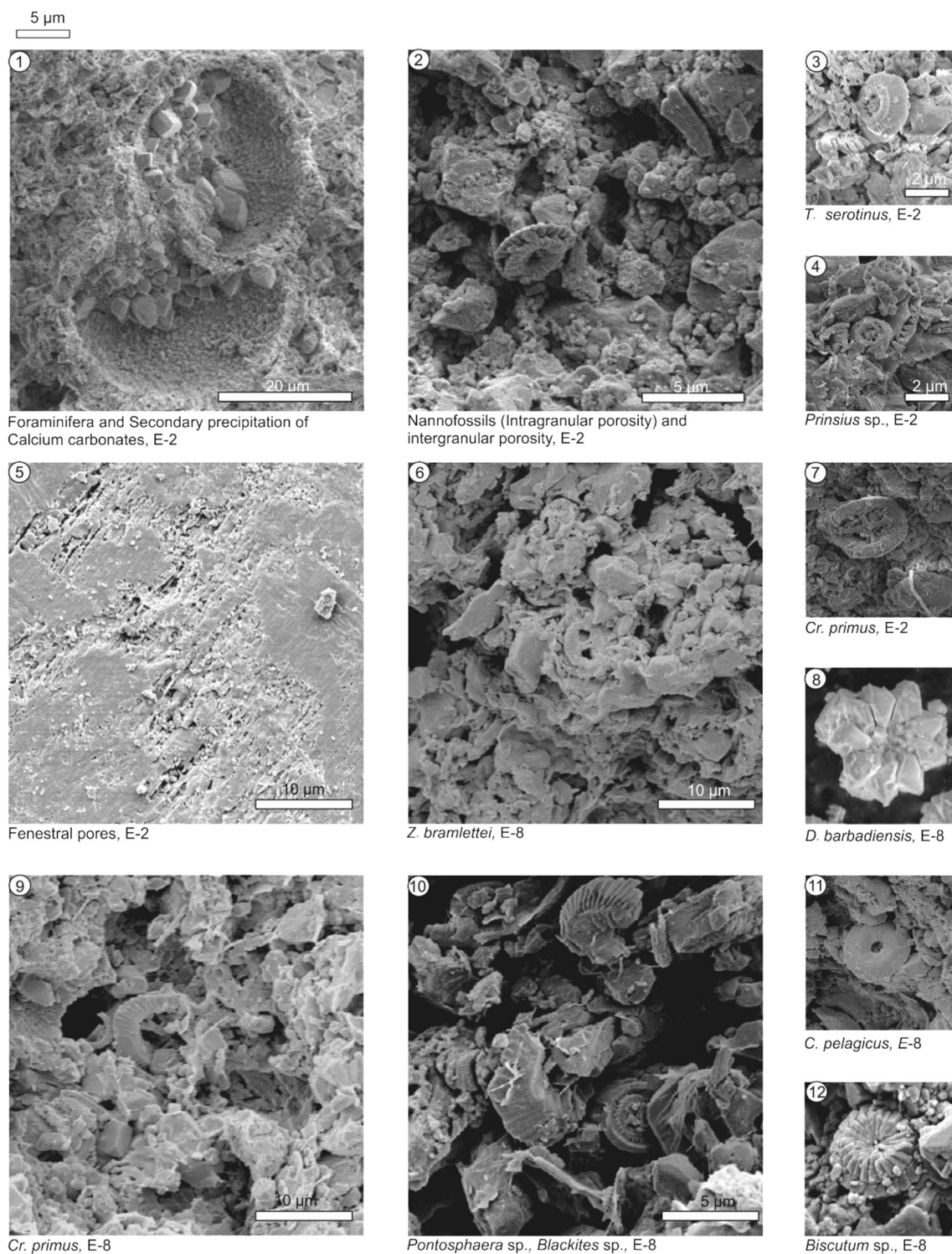


Fig. 6 A plate showing the calcareous nannofossil assemblages found in the studied Paleocene and Eocene strata

fracturing which enhanced the porosity initially; later on, a secondary calcium carbonate precipitated in the fracture space (Fig. 5r). In the same way, a secondary calcium carbonate precipitated also inside the gastropod chambers, thus reducing the porosity of the rock sample (Fig. 5s).

Calcareous nannofossil assemblages and porosity

Calcareous nannofossils are more common in the pelagic settings rather than in the neritic zone. Due to this fact, calcareous nannofossil assemblages are common in the majority of the Eocene samples from E1 to E10, whereas samples E11 and

E12 and those of the Miocene (M1 to M3) are barren. Marker calcareous nannofossil species recognized in the samples such as *T. serotinus* and *D. barbadiensis* assign an early Eocene age for these sediments (Fig. 6-3, and 8).

On a microscale, both intergranular and intragranular pores were observed (Fig. 6-2, 6, 9, and 10), due to the good preservation of microfossils in the deep pelagic settings. Nannofossils, which are defined traditionally by their rims and central area, are commonly empty or have a sieve, cross, or bar shapes. In all aforementioned cases, microporosity still exists if the assemblages are quiet well-preserved or where there is no clay intrusion in the central area (Fig. 6-4, 7, 9, and 11). In few cases, like in *Discoaster* spp., the central area is closed, meaning that no microporosity can be afforded (Fig. 6-8, 10, and 12).

Transport and elastic properties

Measured values of φ , ρ_b , ρ_g , the Klinkenberg permeability, F_1 and F_2 , V_p , V_s , the ν ratio, and the calculated elastic moduli are all listed in Table 2. The measured porosity varies widely from 0.01 to 0.40, with a mean value of 0.23. The lowest-porosity samples (E11 and E12) are grain-supported packstones (nummulitic) enriched in benthic foraminifera with around 20% microcalcite crystals. Although the measured Klinkenberg permeability of the studied samples varies over three orders of magnitude (from 0.005 to 9.013 mD), it is generally low with an average of 0.94 mD. The two low-porosity samples have also the lowest permeability (0.005 and 0.007 mD, respectively). The low permeability originates mainly from the large proportion of micropores and the existence of micritic and microcalcite crystals, which do not contribute effectively to the flow of fluids. The highest porosity was observed in the matrix-supported wackstone facies (Tables 1 and 2).

The bulk and grain densities vary between 1.62 and 2.68, and 2.62 and 2.72, with averages of 2.07 and 2.69 g/cm³, respectively. The unified lithology of the studied rocks is reflected in the very narrow range of the grain density data, whereas the complex diagenetic processes affecting these samples induce wide variations in their porosity and accordingly in their bulk densities. The electrical conductivity data vary over more than three orders of magnitude for a given measurement cycle (Table 2). The calculated values of the formation resistivity factor (F_1 and F_2) are generally small because of the high conductivity of most rock samples induced by their generally moderate/high porosity.

Acoustic wave velocities in the dry samples vary widely from 2281 to 6449 m/s and from 1438 to 3292 m/s for V_p and V_s , respectively (Table 2). The average V_p and V_s are 3878 and 2213 m/s; whereas the average V_p/V_s and ν ratios are 1.71, and 0.23, respectively (Table 2). The ν ratio varies, however, between 0.16 and 0.33, whereas the V_p/V_s ratio varies

from 1.56 to 1.98 (Table 2). The acoustic impedance (AI) of a medium through which the seismic waves are propagating is the product of V_p and ρ_b . It controls the reflectivity of rocks and is an essential parameter in the synthesis of seismic sections and their correlation with the observed seismic profiles (e.g., Soete et al. 2015). It is affected by many parameters such as lithology, porosity, fluids, and pore geometry (Zhang et al. 2012). The V_p and ρ_b data of the dry and water-saturated samples listed in Table 2 result in AI values that vary, respectively, from 3.7 to 17.25×10^6 kg/m².s, and from 3.38 to 17.3×10^6 kg/m².s.

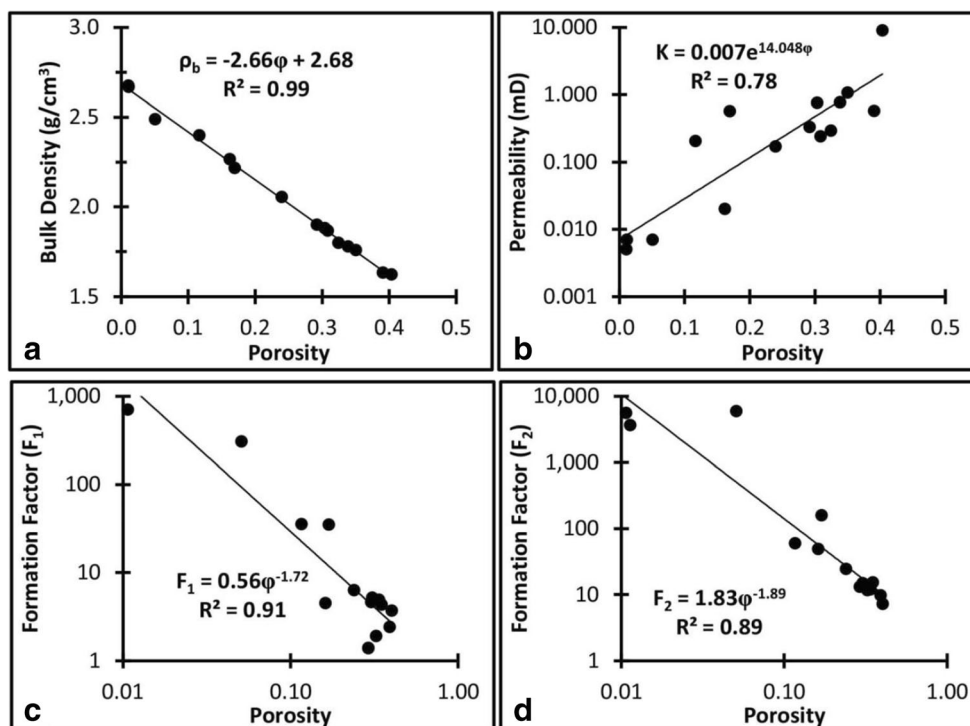
Discussion

Porosity versus other petrophysical properties

Porosity and bulk density are two closely related parameters which are inversely correlated to each other (e.g., Ali et al. 2018). Their robust negative correlation (Fig. 7a) is a good indicator of the reliability of the measurements. On the other hand, porosity is directly proportional to permeability (the poro-perm relationship) with a coefficient of correlation (R^2) of 0.78 (Fig. 7b). The observed slight scatter indicates that, in addition to porosity, there are other factors affecting permeability in carbonate rocks including the grain size, pore volume, pore throat size, and pore geometry. Few samples have different permeabilities at a given porosity such as samples E2 and M1, which have different permeabilities of 0.02 and 0.572 mD, but similar porosities of 0.16 and 0.17, respectively (Table 2, Fig. 7b). Another fact is that although most studied samples are porous, with sometimes porosity of up to 0.40, permeability is generally very low (few fractions of a millidarcy), perhaps because of the small size and the poor connectivity of many pores, as well as the dominance of foraminifera with its *cul-de-sac* (pores closed at one end) porosity. Carbonate rocks have primarily complex pore fabrics and are prone to diagenetic alterations such as dissolution, recrystallization, cementation, and dolomitization, which additionally complicate the poro-perm relationship (Nurmi and Standen 1997; Lapponi et al. 2011; Dewit et al. 2012).

Porosity is strongly correlated with the formation resistivity factor (F_1 and F_2 data) by power relationships and high correlation coefficients (Fig. 7 c, and d). The greater improvement in the electrical conductivity of brine-saturated carbonate rocks (the second run of measurements) is expected if they have negligible clay content or any other electricity-conducting minerals (Casteleyn et al. 2011; Regnet et al. 2015). The obtained average values of the tortuosity (a) factor in the equation $F = a \cdot \varphi^{-m}$ (Archie 1942; Guéguen and Palciauskas 1992) at the two measurement runs are 0.56 and 1.83 while those of the cementation (m) exponent are 1.72 and 1.89, respectively. Regnet et al. (2015) found, in his log-log

Fig. 7 Crossplots of porosity versus bulk density (a), permeability (b), and the formation resistivity factor (F_1 and F_2) calculated from electrical conductivity measurements at two different brine concentrations (c and d)



plot of porosity versus the formation resistivity factor, that the data are not clustered by texture because transmitting properties are greatly affected by the pore diversity even within the same setting. They, however, found a clear clustering by micrite microtextures revealing a strong relationship between micrite properties and micrite morphology. In our study, it is difficult to show such correlation because of the small number of samples.

Permeability and other rock properties

Porosity is inversely correlated with bulk density but directly correlated with permeability, respectively (Fig. 7 a and b). Therefore, an inverse relationship is expected between bulk density and permeability (Fig. 8a). Some scatter in the points is seen, and the correlation coefficient is fair ($R^2 = 0.72$). The difficulty to measure permeability in the field and the relative easiness of measuring the electrical properties have encouraged many researchers to study the relationship between permeability and the formation resistivity factor. The formation resistivity factor is inversely related to permeability usually with a power relationship (e.g., Ravalec et al. 1996; Regnet et al. 2015). According to Walsh and Brace (1984), the two parameters are related as $K \propto F^p$, where $1 \leq p \leq 3$. The values obtained in our study are 0.75 and 0.76, which are very low, indicating the poor correlation between permeability and formation resistivity factor and that estimating permeability from electrical measurements is subject to large possible errors (Regnet et al. 2015). The improvement in the coefficient of correlation from 0.58 at the first run of brine concentration to

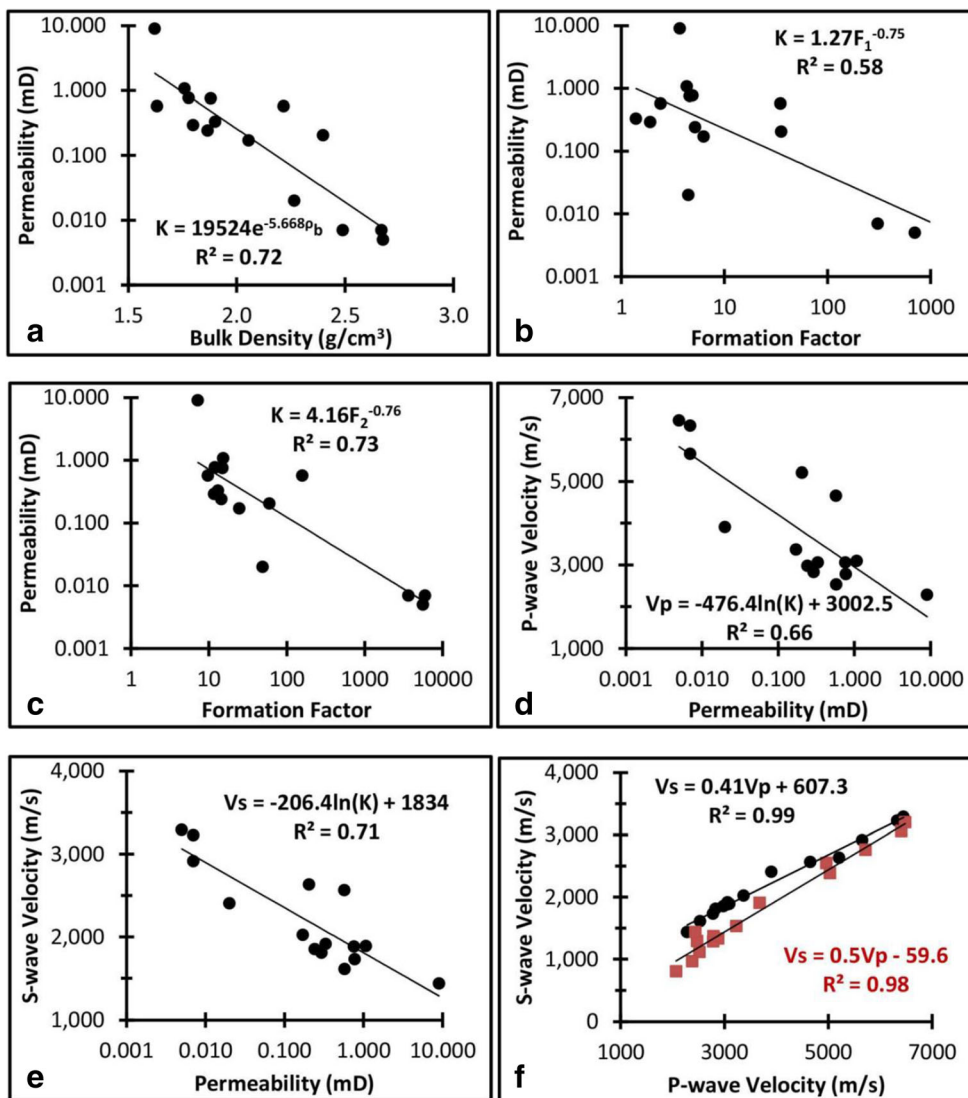
0.73 at the second run (Fig. 8 b and c) points to the effect of factors other than lithology, such as the type and geometry of the pore spaces as well as the fluid nature which dominate the electrical properties of the investigated samples at the higher brine concentration.

Permeability is inversely correlated with the acoustic wave velocities but with fair to moderate correlations (Fig. 8 d and e). Because permeability is sensitive to many other parameters rather than to the total volume of pores only, the relationships between permeability and acoustic wave velocities exhibit higher scatter and lower correlations compared with the φ - V relationship. The measured V_p and V_s for the dry and water-saturated samples are, however, strongly related to each other (Fig. 8f) because they are basically influenced equally by most rock parameters such as lithology, porosity, pore types, and shapes although they may respond differently to the fluid type and degree of saturation. Both relationships have higher correlations indicating the consistency of the measurements. For a given dry rock sample, the V_s is 57% of the corresponding V_p value but decreased to only 48% of the corresponding V_p after saturation (Table 2; Fig. 8F). This is induced mainly by the stronger reduction of shear wave velocities under saturation conditions (Anselmetti et al. 1997; Kearey et al. 2002; Verwer et al. 2008).

Capillary imbibition

It is not easy to achieve complete saturation when conducting capillary imbibition tests because the driving mechanism of the capillary front in substances with pores of variable sizes

Fig. 8 Crossplots of bulk density versus permeability (a); formation resistivity factors versus permeability (b and c); permeability versus acoustic wave velocities (d and e); and between V_p and V_s of the dry (solid circles) and water-saturated (colored squares) samples (f)



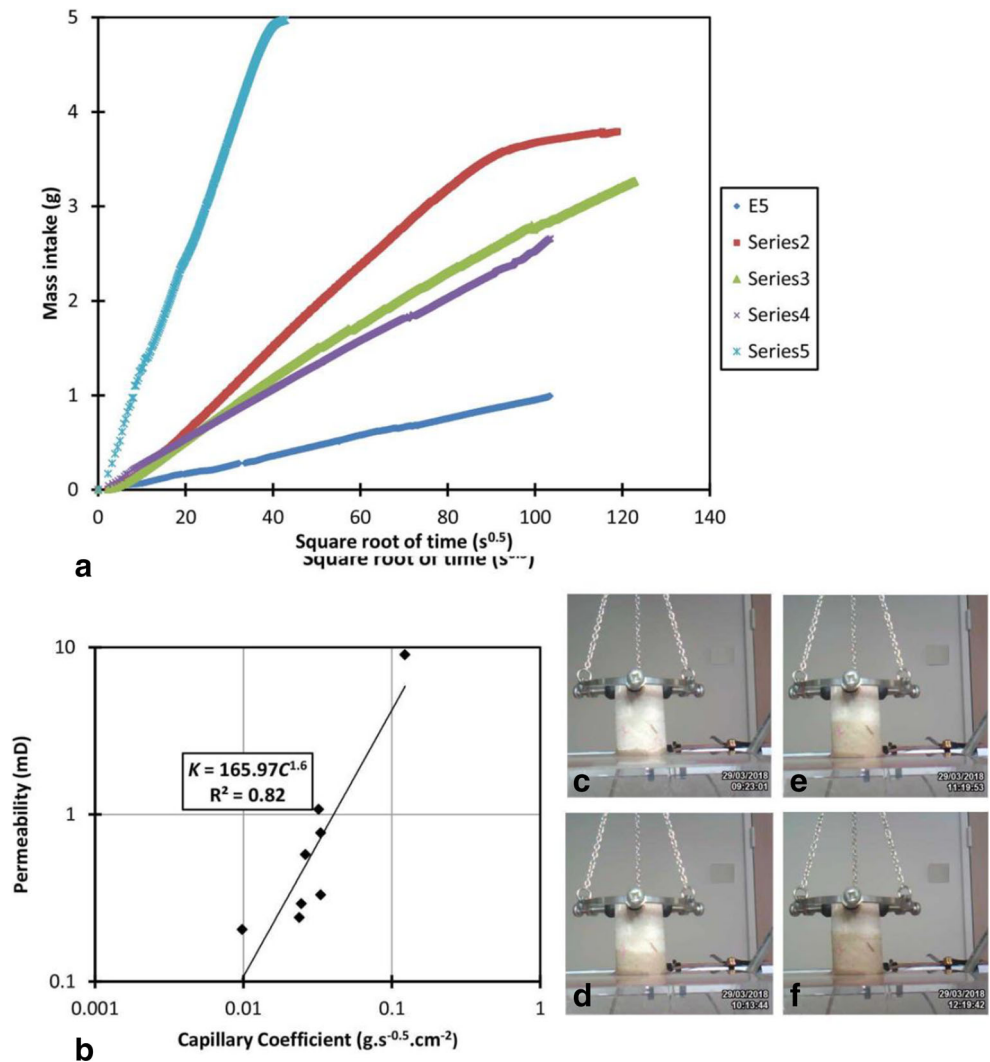
induces air trapping. Thus, estimating the exact amount of saturation (by water) in the middle phases is not that easy. In contrast, it is much easier to obtain the overall saturation when the front of water reaches the topmost end of the investigated core (David et al. 2015). As stated before, we measured the mass increase (due to water intake) with time for eight samples then plot the mass intake versus radical time data to calculate the coefficient of capillarity C . The imbibition curves of five plugs are illustrated in Fig. 9a, revealing the direct proportionality between the mass intake and the square root of time. The obtained coefficient of capillarity C , the strength of the fit judged from the value of the coefficient of correlation, porosity, and permeability of the tested samples are listed in Table 3. The final saturation at the end of the experiment is also reported. In their study of the X-ray imaging of water motion during capillary imbibition in porous media, David et al. (2011) predicted a positive relationship between the capillarity coefficient (C) and permeability (K) because both of them are controlled by

the motion of fluids in the connected pore network of the material. The obtained relationship is illustrated in Fig. 9b where a direct trend is observed between the two parameters which are related to each other as $K = 165.97C^{1.6}$ ($R^2 = 0.82$). The gradually rising water front is monitored during the experiment as shown for sample 9 in Fig. 9c–f. Recently, Benavente et al. (2015) have arrived to an analogous relationship, which uses both the capillary coefficient and the rock microstructural parameters to calculate permeability as:

$$K = C^2 \cdot \eta r / 4 \varphi \rho^2 \gamma \cos \theta.$$

This equation includes information on water flow rate (the coefficient of capillarity C), water properties (viscosity η and density ρ), wetting condition (interfacial tension γ and the angle of contact θ), and pore structure (porosity φ and radius r of the pore). If these parameters are accurately known, a better correlation between permeability and the capillarity coefficient could be obtained. The scatter in our plot (Fig. 9b) and the moderate correlation coefficient are indeed induced by

Fig. 9 (a) Water mass intake evolution of five carbonate samples as a function of the square root of time and (b) the relationship between the coefficient of capillarity and permeability of the studied eight samples. Height evolution of the water front across sample E9 at different time intervals (c–f). The experiment started at 09:19:31 am and ended at 13:31:51 (i.e., lasted for 4 h, 12 min, and 20 s)



the variability of these parameters especially porosity and the pore radii. This possibility of predicting important rock parameters from simple experiments justifies the new interest in introducing the inexpensive capillary imbibition tests in the lab (David et al. 2015).

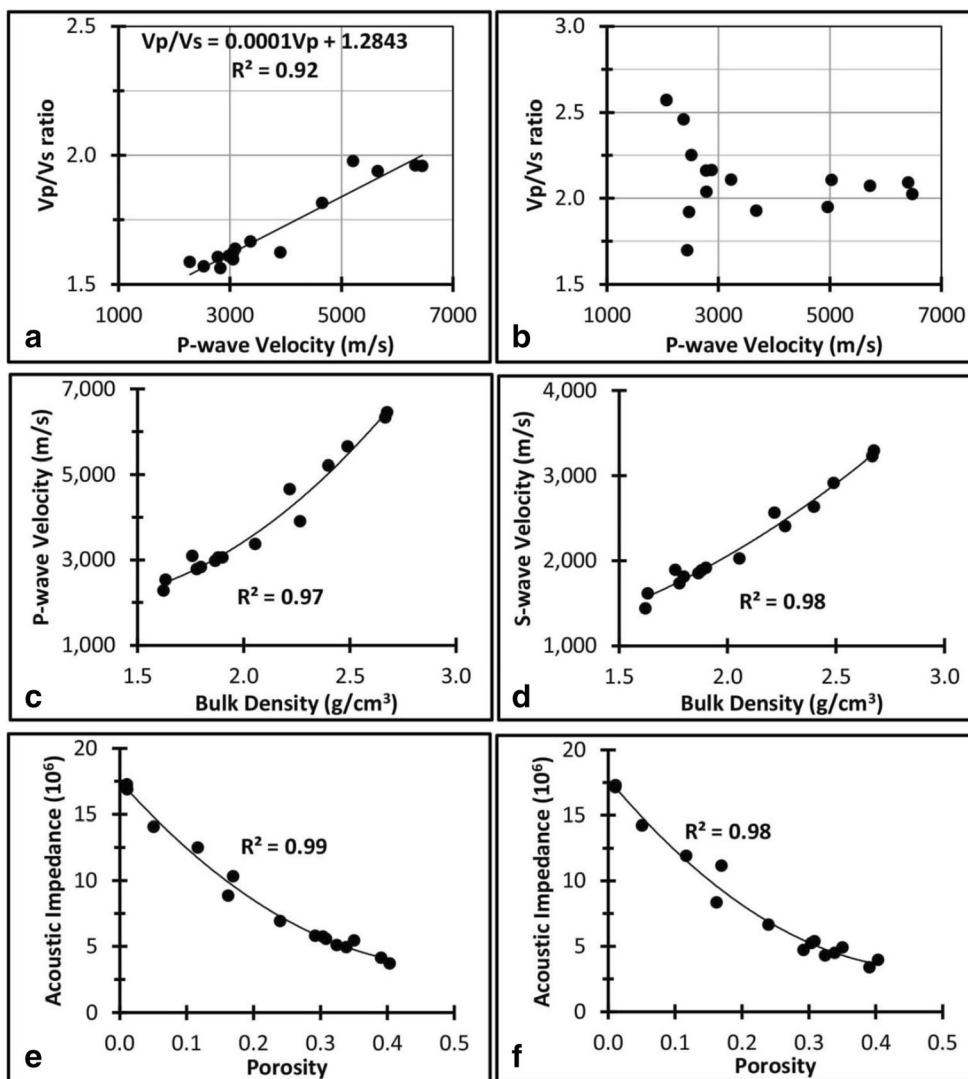
Acoustic velocities and porosity

The relationship between V_p and the V_p/V_s ratio is shown in Fig. 10a. The obtained V_p/V_s and the ν ratios (Table 2) are in general lower than the commonly observed values for

Table 3 Petrophysical properties and coefficient of capillarity “C” of 8 selected samples obtained with the mass intake method

Sample No.	Porosity	Permeability (mD)	Mass intake results			
			C (g/s ^{1/2} /cm ²)	Corr. coeff.	Saturation (%)	Linearity quality
E1	0.31	0.242	0.0238	0.981	74.92	Bumpy
E3	0.29	0.331	0.0332	0.991	52.03	Poor beginning-bumpy
E4	0.35	1.072	0.0321	0.998	76.45	Good beginning-bumpy
E5	0.12	0.205	0.0098	0.998	19.05	Good linearity
E6	0.34	0.774	0.0332	0.951	66.71	Excellent
E9	0.39	0.576	0.0262	0.993	41.22	Good beginning-bumpy
E10	0.32	0.293	0.0246	0.998	53.91	Good beginning-bumpy
M2	0.40	9.013	0.1227	0.995	79.08	Good

Fig. 10 Crossplots of V_p versus the V_p/V_s ratio of the dry (a) and water-saturated (b) samples; ρ_b versus V_p and V_s (c and d); and φ versus the acoustic impedance (AI) of the dry (e) and water-saturated (f) samples

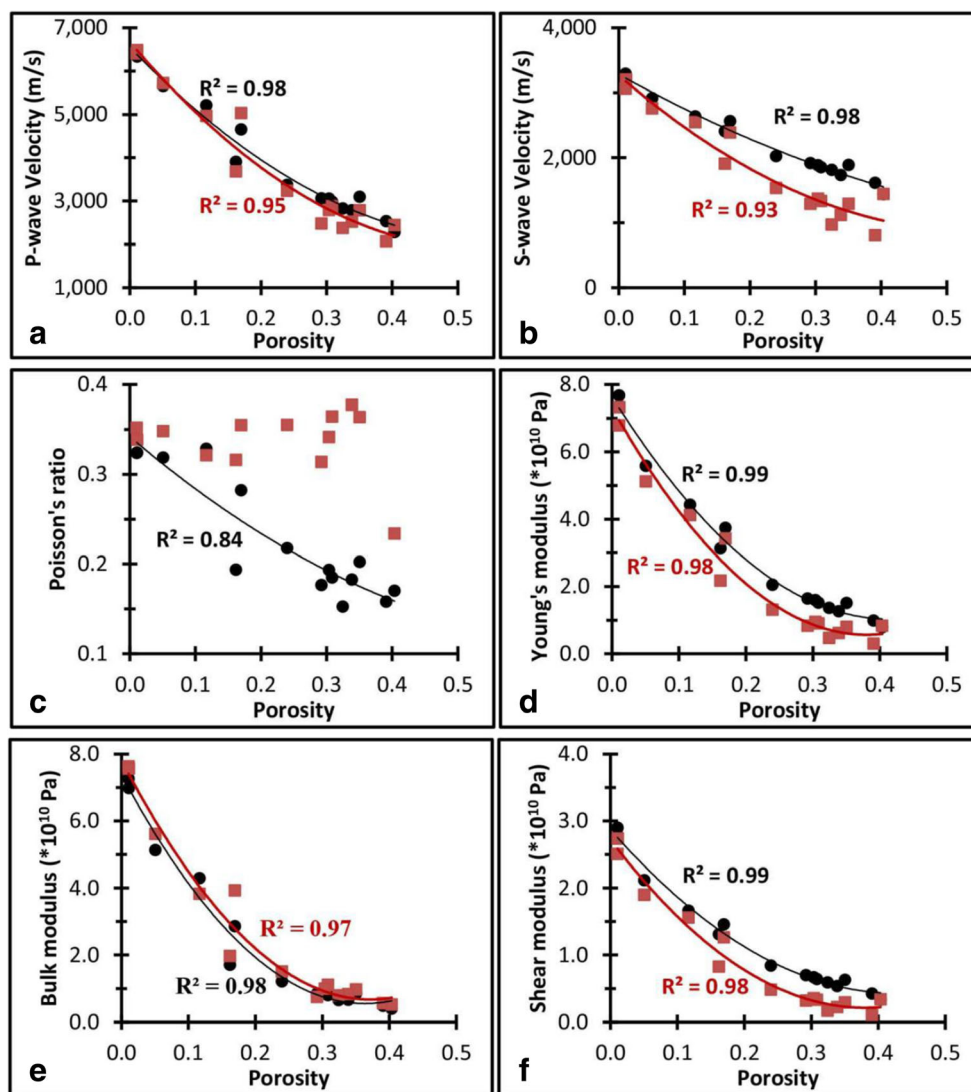


limestones ($\nu=0.3$; Schlumberger 2013) and may result from the existence of crystalline, rather than granular, textures in the studied carbonate rocks (Verwer et al. 2008). This inference is supported by the petrographic study which indicates the dominance of crystalline textures in the studied samples (Figs. 4, and 5). Upon saturation, a great decrease in the shear wave velocity was observed, where the average V_p and V_s are 3723 and 1801 m/s (Fig. 8f) and averages V_p/V_s and ν ratios of 2.10 and 0.35, respectively. In this case, the V_s value is only 48% of the V_p value of the water-saturated sample. The V_p/V_s ratios of the water-saturated samples vary widely between 1.70 and 2.57 (Fig. 10b) compared with only from 1.56 to 1.98 for the dry samples. The higher V_p/V_s and ν ratios of the water-saturated rocks are induced mainly by the greater drop in the shear wave velocity. Although the V_p of the water-saturated samples are generally higher than those of the dry rocks, some previous results revealed a mixed behavior whereby the V_p may increase or decrease with saturation (e.g., Verwer et al. 2008). Such behavior was also observed for our samples (Table 2).

Acoustic velocities are strongly dependent on bulk densities (Kearey et al. 2002) where velocities generally display linear increase with increasing density and decreasing porosity (e.g., Verwer et al. 2008; Ali et al. 2018), a fact that is clearly supported by the strong positive correlation between ρ_b and both the V_p and V_s of the presently investigated samples (Fig. 10 c and d). On the other hand, the AI, calculated for the dry and water-saturated rocks, is inversely related to porosity with strong correlations (Fig. 10 e and f).

Total porosity plays the major role in controlling the seismic wave velocity in rocks of similar mineralogical composition where both V_p and V_s decrease with increasing porosity (e.g., Verwer et al. 2008; Regnet et al. 2015). Similar to the usually observed concave-upward trends between porosity and acoustic velocity (Neto et al. 2015), our seismic velocity data display inverse polynomial trends with porosity (Fig. 11 a and b). Velocity variation at a given porosity is higher for the water-saturated samples than for the dry rocks. The good fit of the V - φ relationship and the low/moderate dispersion of

Fig. 11 Crossplots of φ versus V_p of the dry (solid circles) and water-saturated (colored squares) samples (**a**); φ versus V_s of the dry (solid circles) and water-saturated (colored squares) samples (**b**); φ versus ν ratio of the dry (solid circles) and water-saturated (colored squares) samples (**c**); φ versus Young's modulus of the dry (solid circles) and water-saturated (colored squares) samples (**d**); φ versus bulk modulus of the dry (solid circles) and water-saturated (colored squares) samples (**e**); and φ versus shear modulus of the dry (solid circles) and water-saturated (colored squares) samples (**f**)



velocity data at a given porosity have also been observed in previous studies (e.g., Baechle et al. 2008; Fournier et al. 2011), although the exact pattern may differ for a larger number of samples. Few samples, especially the water saturated, display different seismic velocities at a given porosity. For example, samples E2 and M1 have similar porosities of 0.162 and 0.169 but differ largely in their V_p which are 3903 and 4654 m/s, respectively (Table 2, Fig. 11a) even though both are grain-supported packstones (Table 1). This behavior has also been observed by other researchers and arises possibly due to different pore types in the carbonate rock (Eberli et al. 2003). Pores occurring in a rigid rock framework induce higher velocities than interparticle pores, for example.

Tightly cemented marine carbonate grainstones with significant amounts of micropores (Fournier et al. 2011, 2014) show lower seismic wave velocities at a given porosity compared with travertines (Soete et al. 2015), which are deposited

in thin water films under greatly variable sub-aerial conditions. Previous studies revealed that not only porosity, but also pore types and shapes, affect the seismic velocity in carbonate rocks, and any increase in the proportion of micropores reduces the velocity at a given porosity. On the other hand, stiff (such as mouldic) pores would induce a more rigid framework and thus higher seismic velocity at a given porosity (Anselmetti et al. 1997; Eberli et al. 2003; Weger et al. 2009; Xu et al. 2009).

For the dry samples, the calculated ν ratio is inversely related to porosity with a high coefficient of correlation (Fig. 11c). Verwer et al. (2008) noticed that the highest porosity rocks have Poisson's ratios lower than 0.28, which is consistent with our observations. Neto et al. (2015) found also an inverse relationship between porosity and the V_p/V_s ratio of a suite of carbonate rocks from Brazil. Samples showing this behavior are characterized by high-porosity recrystallized textures with a frame that is supporting the shear wave

propagation. The ν ratio of the water-saturated samples increases significantly (Table 2 and Fig. 11c) because of the large decrease in V_s with saturation especially at higher porosities. A similar behavior has also been observed for the Neogene carbonates and siliciclastics from the subsurface of the Florida Keys by Anselmetti et al. (1997), revealing the higher V_s sensitivity to the induced shear weakening.

Porosity is inversely related to the elastic moduli of the dry and water-saturated samples (Fig. 11 d, e, and f). They are related to each other by polynomial trends that are clearly concave upward. In addition, there is a clear decrease in the values of Young's and shear moduli of the water-saturated samples (Fig. 11 d and f), although the Gassmann's theory assumes that the shear modulus remains essentially the same during fluid substitution. Results obtained in this study as well as other previous studies (e.g., Adam et al. 2006) indicate that this does not apply for limestones. The rocks are usually influenced by rigidity changes (up or down), hence restricting the application of Gassmann's theory to predict the seismic wave speeds in carbonate rocks. The shear modulus decreases with saturation in granular carbonate rocks but increases in crystalline and cemented carbonates (Verwer et al. 2008). Therefore, the elastic properties of a carbonate rock alone may enable a quick estimation of its granular or crystalline texture and can help in predicting the rock nature from seismic data acquired across boreholes. On the other hand, values of the bulk moduli have slightly increased upon saturation (Fig. 11e).

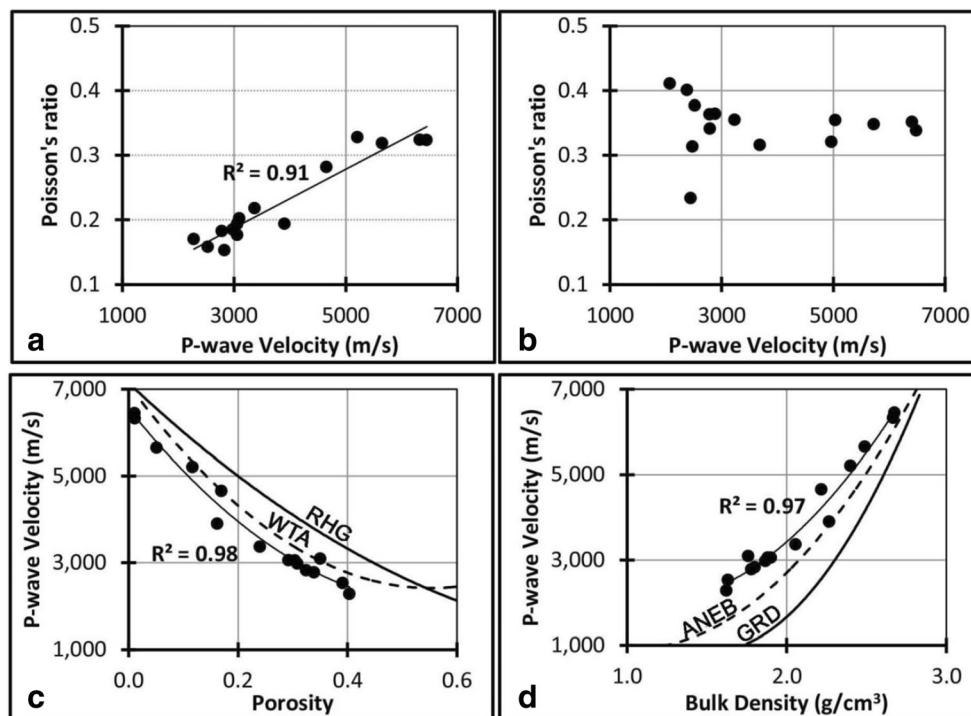
In addition to porosity, acoustic velocities in carbonate rocks are controlled also both by the depositional lithology and the subsequent diagenetic alterations (Verwer et al. 2008). In this way, primary fabrics may be quickly overprinted by diagenetic changes such as recrystallization and cementation. Most of the matrix-supported wackstones have higher porosities and lower seismic wave velocities. On the other hand, samples E5, E11, E12, M1, and M3 have higher-than-average seismic velocities and are either matrix-supported wackstone/packstone or grain-supported packstones. Verwer et al. (2008) used the texture class assignment proposed by Kenter et al. (2007), whether granular or crystalline, to relate particular ranges of diagnostic acoustic velocities for each texture. Granular textures refer to depositional grains where grain-to-grain contacts support the rock framework. Rocks with granular textures have little matrix or cement and result typically in low V_p , relatively low V_s , and higher ν ratios under saturation conditions. Rocks with crystalline textures have been recrystallized or cemented after deposition and have altered their original grain-dominated fabric to a crystal-dominated one. These rocks have generally low to high V_p , high V_s , resulting in low ν ratios. Highly cemented, sparite-forming and intensive secondary crystal-fill samples of low porosity and higher seismic wave velocity such as E5, E11, E12, M1, and M3 belong to this category (Tables 1 and 2).

Mineralogy and the ν ratio in carbonate rocks

The mineral composition has a larger impact on velocity variations in siliciclastic sediments which exhibit wide variations in mineralogy from quartz to clay, than in carbonates (Christensen and Szymanski 1991; Braaksma et al. 2003). Consistent with earlier findings of Anselmetti and Eberli (1993), Verwer et al. (2008) found no significant effect of the dolomite fraction on the measured seismic velocities of carbonates which indicate that the observed variations in seismic velocities are induced mainly by the rock texture rather than variations in mineralogy. Based on the results of Anselmetti and Eberli (1993, 2001) and Kenter et al. (2002), porosity is the main control on the seismic velocity of carbonate rocks, although pore type and the percentage of micropores play also a role and this is why some rocks have different velocities at a given porosity. However, the details of the coupling between pore types and seismic velocity are not straightforward and very difficult to quantify, in contrast to those of the φ - V relationship, because pore type characterization is a qualitative process and because many pores are combinations of different types and their description remains subject to interpretation (Lønøy 2006; Verwer et al. 2008). Increasing quartz content reduces the acoustic velocities of the carbonate rocks because it resists dissolution, hindering cementation and the associated increase of the seismic wave velocities. On the other hand, acoustic wave velocities increase slightly with increasing dolomite content.

Verwer et al. (2008) evaluated the specific effects of rock texture on a crossplot of V_p and the ν ratio. Samples which plot in the lower left of the plot (with $V_p < 4500$ m/s and ν ratio < 0.28) have granular textures, whereas samples located on the remaining space of the plot ($V_p > 4500$ m/s and ν ratio > 0.28 or $V_p < 4500$ m/s and ν ratio > 0.28) have crystalline textures. In this way, we can distinguish the samples of granular textures (E1, E2, E3, E4, E6–E10, and M2) from those of crystalline textures (E5, E11, E12, M1, and M3) on the plot of V_p versus the ν ratio (Fig. 12a). Moreover, the crossplot of V_p versus ν ratio for the saturated samples displays a V-shaped cluster in which the granular textures occupy the upper part of the left wing, whereas the crystalline textures occupy the lower left and the right wing of the crossplot (Fig. 12b). This means that rocks of granular textures show large increase of ν ratio upon saturation with a mean value of 0.15, whereas rocks of the crystalline textures show only slight ν ratio increase (Verwer et al. 2008). The transition between the granular and crystalline textures occurs at a V_p of 4500 m/s and a ν ratio of 0.28. Early diagenesis and compaction of rocks having granular textures increase their V_p and decrease their ν ratio (e.g., Wilkens et al. 1984). With further maturation and cementation, the V_p will increase accompanied by a slight increase of ν ratio. Toward zero porosity (high cementation and high V_p), the ν ratio of carbonate

Fig. 12 Crossplots of V_p versus the ν ratio of the dry (a) and water-saturated (b) samples. Plots of φ versus V_p (c) and ρ_b versus V_p (d) are shown with the models of WTA, RHG, GRD, and ANEB superimposed (see text for details)



rocks is approximated by the ν ratio of pure calcite and dolomite at 0.31 and 0.29, respectively (Simmons and Wang 1971). Therefore, samples E11 and E12 (grain-supported packstone) have very low porosity (1.1%), high V_p (above 6300 m/s), and high ν ratios of 0.32. The processes of dolomitization, recrystallization, dissolution, and cementation have differential impacts on the V_p and V_s and, accordingly, on the ν ratio as explained in detail by Verwer et al. (2008). Any diagenetic process may act on a rock whose V_p and ν ratio have a certain position on the plot, but each process has its specific trend on the path (Anselmetti and Eberli 2001).

In order to compare the presently obtained trend between porosity and velocity with previous results, we plot our data superimposed on the trends obtained by the Raymer-Hunt-Gardner (RHG) model (Raymer et al. 1980) and the Wyllie's time average (WTA) equation (Wyllie et al. 1956, 1958) in Fig. 12c. In addition, the density-velocity trends of Gardner et al. (1974) (GRD) and Anselmetti and Eberli (1993) (ANEB) equations are also superimposed on the crossplot of bulk density versus velocity (Fig. 12d). At a given porosity, velocities obtained in our study are lower than those of the RHG model but close to the results of the WTA equation. On the other hand, the obtained velocities are higher than velocities of the GRD model but closer the results of ANEB at a given bulk density. In general, depositional conditions, composition, the sequence of diagenetic alterations, and the subsequent deformation are all factors leading to the observed differences (Anselmetti and Eberli 1993, 2001; Eberli et al. 2003; Verwer et al. 2008).

Conclusions

Transport and elastic properties (porosity, density, permeability, electrical conductivity, and acoustic velocities) coupled with thin sections, calcareous nannofossil, and SEM investigations were conducted on fifteen carbonate samples collected from the Paleogene strata exposed at Zahle, central Lebanon. The electrical conductivity was tested in two successive runs of different brine concentrations, whereas the acoustic wave velocities were measured for the dry and water-saturated samples. We also examined the self-imbibition of selected samples by monitoring the moving capillary front across a sample. From the measured properties, we further calculated other petrophysical and elastic parameters such as the formation resistivity factor, the cementation exponent, the V_p/V_s and ν ratios, the acoustic impedance, as well as the rocks' elastic moduli. This integrated analysis provides a deep insight into the different parameters controlling the petrophysical and elastic behavior of the investigated rocks.

Porosity is negatively and positively correlated with bulk density and permeability, respectively. Imbibition experiments showed good linear fits between the mass increase and the square root of time. The resulting capillary coefficients exhibit good correlation with permeability. Although porosity has the major control on both the transport (permeability and electrical conductivity) and elastic properties of the studied rocks, the amount of microporosity plays a role as well. Acoustic velocities decrease with the increase in porosity because the ultrasonic wave propagation is impeded in porous

media. On average, the shear wave velocity is 57% and 48% of the primary wave velocity of a sample under dry and water-saturation condition, respectively, revealing the great drop in the values of the shear modulus of rocks with saturation and the consequent increase of the V_p/V_s and ν ratios.

Some samples in this study display different seismic wave velocities at equal porosities indicating that in addition to porosity, pore types, sizes, and shapes as well as the rock diagenetic history control also the acoustic wave velocities. Higher velocities may result not only from lower porosity but also from the development of stiff and cohesive micrite microstructures. In addition, velocity increase may also result from increase of grain size and growing contact cementation. Grain size, packing, matrix, cement, and the crystal shapes are therefore additional factors controlling the propagation velocity of seismic waves in carbonate rocks. Acoustic impedance data of both the dry and water-saturated samples vary widely because of the wide variations in the dry ρ_b and the V_p . Therefore, seismic reflection sections in carbonate sequences may contain reflections produced from different pore types and shapes rather than the existence of intercalations of other non-carbonate minerals. The present study revealed also that seismic measurements such as the changes in the shear modulus and hence the V_p/V_s and ν ratios with saturation are useful tools for discriminating between the different textures of carbonate rocks. The ability to extract the rock texture from seismic measurements allows the prediction of porosity types and its evolution from sonic logs acquired for similar sediments.

Results obtained in this study give a deeper insight into the understanding and interpretation of the various petrophysical properties of microporous rocks which are valuable in seismic-based exploration and evaluation of marine platform carbonate rocks. However, more detailed petrographic and pore fabric analyses, coupled with petrophysical and acoustic measurements on a large number of dry and water-saturated core samples, are required for deeper understanding of the nature of these rocks and for extending the obtained results to the interpretation of the seismic profiles acquired above the corresponding subsurface occurrences of the studied formations.

Funding information This research has been partially financed through a URB (University Research Board) Grant from the American University of Beirut (Award No. 103009; Project No. 22759).

References

- Adam L, Batzle M, Brevik I (2006) Gassmann's fluid substitution and shear modulus variability in carbonates at laboratory seismic and ultrasonic frequencies. *Geophys* 71(6):F173–F183
- Ali A, Wagreeh M, Strasser M (2018) Depositional constraints and diagenetic pathways controlling petrophysics of middle Miocene shallow-water carbonate reservoirs (Leitha limestones), Central Paratethys, Austria-Hungary. *Mar Pet Geol* 91:586–598. <https://doi.org/10.1016/j.marpetgeo.2018.01.031>
- Alqudah M, Monzer A, Sanjuan J, Salah MK, Alhejoj IK (2019) Calcareous nannofossil, nummulite and ostracod assemblages from Paleocene to Miocene successions in the Bekaa Valley (Lebanon) and its paleogeographic implications. *J Afr Earth Sci* 151:82–94. <https://doi.org/10.1016/j.jafrearsci.2018.12.001>
- Alsharhan AS, Nairn AEM (1995) Tertiary of the Arabian Gulf: sedimentology and hydrocarbon potential. *Palaeogeogr Palaeoclimatol Palaeoecol* 114:369–384
- Anselmetti FS, Eberli GP (1993) Controls on sonic velocity in carbonates. *PAGEOPH* 141:287–323
- Anselmetti FS, Eberli GP (1999) The velocity-deviation log: a tool to predict pore type and permeability trends in carbonate drill holes from sonic and porosity or density logs. *AAPG Bull* 83:450–466
- Anselmetti FS, Eberli GP (2001) Sonic velocity in carbonates—a combined product of depositional lithology and diagenetic alterations, in R. N. Ginsburg, ed., *Subsurface geology of a prograding carbonate platform margin, Great Bahama Bank, results of the Bahamas drilling project*. *Soc Sed Geol* 70:193–216
- Anselmetti FS, von Salis GA, Cunningham KJ, Eberli GP (1997) Acoustic properties of Neogene carbonates and siliciclastics from the subsurface of the Florida Keys: implications for seismic reflectivity. *Mar Geol* 144:9–31
- Archie GE (1942) Electrical resistivity log as an aid in determining some reservoir characteristics. *Trans AIME* 146:54–62
- Baechele G, Colpaert A, Eberli G, Weger R (2008) Effects of microporosity on sonic velocity in carbonate rocks. *Lead Edge* 27:1012–1018
- Benavente D, Pla C, Cueto N, Galvan S, Martinez-Martinez J, Garcia-del-Cura MA, Ordóñez S (2015) Predicting water permeability in sedimentary rocks from capillary imbibition and pore structures. *Eng Geol* 195:301–311. <https://doi.org/10.1016/j.enggeo.2015.06.003>
- Beydoun ZR (1991) Arabian plate hydrocarbon, geology and potential - a plate tectonic approach. *AAPG Stud Geol* 33:77
- Beydoun ZR (1999) Evolution and development of the Levant (Dead Sea Rift) transform system: a historical-chronological review of a structural controversy, in MacNiocail C & Rayan PD (eds), *Continental tectonics*. *Geol Soc Lond special pub* 164: 239–255
- Biddle KT, Schlager W, Rudolph KW, Bush TL (1992) Seismic model of a progradational carbonate platform, Picco di Valandro, the Dolomites, northern Italy. *AAPG Bull* 76:14–30
- Biot MA (1956a) Theory of propagation of elastic waves in a fluid saturated porous solid—I: low frequency range. *J Acoust Soc Am* 28: 168–178
- Biot MA (1956b) Theory of propagation of elastic waves in a fluid saturated porous solid—II: high frequency range. *J Acoust Soc Am* 28: 179–191
- Braaksma H, Kenter JAM, Proust JN, Dijkmans V, Van Hoek T, Mahieux G, Drijkoningen GG (2003) Case history controls on acoustic properties of Upper Jurassic siliciclastic rocks (Boulonnais, northern France). *Geophys* 68(1):58–69
- Brigaud B, Vincent B, Durlot C, Deconinck J-F, Blanc P, Trouiller A (2010) Acoustic properties of ancient shallow-marine carbonates: effects of depositional environments and diagenetic processes (Middle Jurassic, Paris Basin, France). *J Sediment Res* 80:791–807
- Burchette TP (2012) Carbonate rocks and petroleum reservoirs: a geological perspective from the industry. *Geol Soc Lond Spec Publ* 370: 17–37. <https://doi.org/10.1144/SP370.14>
- Campbell AE, Stafleu J (1992) Seismic modeling of an Early Jurassic, drowned carbonate platform: Djebel Bou Dahar, High Atlas, Morocco (1). *AAPG Bull* 76:1760–1777
- Casteleyn L et al (2010) Interrelations of the petrophysical, sedimentological and microstructural properties of the Oolithe Blanche formation (Bathonian, saline aquifer of the Paris Basin). *Sediment Geol* 230:123–138. <https://doi.org/10.1016/j.sedgeo.2010.07.003>

- Casteleyn L, Robion P, David C, Collin PY, Menéndez B, Fernandes N, Desaubliaux G, Rigollet C (2011) An integrated study of the petrophysical properties of carbonate rocks from the “Oolithe Blanche” formation in the Paris Basin. *Tectonophysics* 503:18–33
- Christensen NI, Szymanski DL (1991) Seismic properties and the origin of reflectivity from a classic Paleozoic sedimentary sequence, valley and ridge province, southern Appalachians. *Geol Soc Am Bull* 103:277–289
- David C, Menéndez B, Mengus J-M (2008) The influence of mechanical damage on the fluid flow patterns investigated using CT scanning imaging and acoustic emissions techniques. *Geophys Res Lett* 35:L16313. <https://doi.org/10.1029/2008GL034879>
- David C, Menéndez B, Mengus J-M (2011) X-ray imaging of water motion during capillary imbibition in porous rocks. Part 1: methods, microstructures and mechanical deformation. *J Geophys Res* 116:B03204. <https://doi.org/10.1029/2010JB007972>
- David C, Bertauld D, Dautriat J, Sarout J, Menéndez B, Nabawy B (2015) Detection of moving capillary front in porous rocks using X-ray and ultrasonic methods. *Front Phys* 3:53. <https://doi.org/10.3389/fphy.2015.00053>
- Deville de Periere M, Durllet C, Vennin E, Lambert L, Bourillot R, Caline B, Poli E (2011) Morphometry of micrite particles in cretaceous microporous limestones of the Middle East: influence on reservoir properties. *Mar Pet Geol* 28:1727–1750. <https://doi.org/10.1016/j.marpetgeo.2011.05.002>
- Dewit J, Huysmans M, Muchez P, Hunt DW, Thurmond JB, Verges J, Saura E, Fernandez N, Romaine I, Esestine P, Swennen R (2012) Reservoir characteristics of fault-controlled hydrothermal dolomite bodies: Ramales platform case study. *Geol Soc Lond Spec Publ* 370(1):83–109
- Dürrast H, Siegesmund S (1999) Correlation between rock fabrics and physical properties of carbonate reservoir rocks. *Int J Earth Sci* 88:392–408
- Eberli G, Baechle G, Anselmetti F, Incze M (2003) Factors controlling elastic properties in carbonate sediments and rocks. *Lead Edge* 22(7):654–660
- Ehrenberg SN, Aqrabi AAM, Nadeau PH (2008) An overview of reservoir quality in producing cretaceous strata of the Middle East. *Pet Geosci* 14:307–318
- Fabricius IL (2003) How burial diagenesis of chalk sediments controls sonic velocity and porosity. *AAPG Bull* 87(11):1755–1778
- Fabricius IL, Røgen B, Gommessen L (2007) How depositional texture and diagenesis control petrophysical and elastic properties of samples from five North Sea chalk fields. *Pet Geosci* 13:81–95
- Folk RL (1966) A review of grain-size parameters. *Sedimentol* 6:73–93
- Fournier F, Leonide P, Biscarrat K, Gallois A, Borgomano J, Foubert A (2011) Elastic properties of microporous cemented grainstones. *Geophys* 76:E211–E226. <https://doi.org/10.1190/geo2011-0047.1>
- Fournier F, Leonide P, Kleipool L, Toullec R, Reijmer JJJ, Borgomano J, Klootwijk T, Van Der Molen J (2014) Pore space evolution and elastic properties of platform carbonates (Urgonian limestone, Barremian-Aptian, SE France). *Sediment Geol* 308:1–17
- Gardner GHF, Gardner LW, Gregory AR (1974) Formation velocity and density—the diagnostic basics for stratigraphic traps. *Geophys* 39:770–780
- Gassmann F (1951) Elastic waves through a packing of spheres. *Geophys* 16:673–685
- Gerçek H (2007) Poisson's ratio values for rocks. *Int J Rock Mech Min Sci* 44:1–13
- Guéguen Y, Palciauskas V (1992) Introduction to the physics of rocks. Princ Univ Press, Princeton
- Hudson JA, Cosgrove JW, Kemppainen K, Johansson E (2011) Faults in crystalline rock and the estimation of their mechanical properties at the Olkiluoto site, western Finland. *Eng Geol* 117:246–258
- Kaldi J (1989) Diagenetic microporosity (chalky porosity), Middle Devonian Kee Scarp reef complex, Norman Wells, Northwest Territories, Canada. *Sediment Geol* 63:241–252
- Kearey P, Brooks M, Hill I (2002) An introduction to geophysical exploration. Blackwell Pub
- Kenter J, Podladchikov F, Reinders M, Van der Gaast S, Fouke B, Sonnenfeld M (1997) Parameters controlling sonic velocities in a mixed carbonate-siliciclastics Permian shelf-margin (upper San Andres formation, Last Chance Canyon, New Mexico). *Geophys* 62:505–520
- Kenter JAM, Anselmetti FS, Kramer PH, Westphal H, Vandamme MGM (2002) Acoustic properties of “young” carbonate rocks, ODP leg 166 and boreholes Clino and Unda, Western Great Bahama Bank. *J Sediment Res* 72:129–137
- Kenter J, Braaksma H, Verwer K, van Lanen X (2007) Acoustic behavior of sedimentary rocks: geologic properties versus Poisson's ratios. *Lead Edge* 26:436–444
- Khazanehdari J, Sothcott J (2003) Variation in dynamic shear elastic modulus of sandstone upon fluid saturation and substitution. *Geophys* 68:472–481
- Klinkenberg LJ (1941) The permeability of porous media to liquids and gases. *Am Pet Inst, Drill Prod Pract*:200–213
- Lapponi F, Casini G, Sharp I, Blendinger W, Fernandez N, Romaine I, Hunt D (2011) From outcrop to 3D modelling: a case study of a dolomitized carbonate reservoir, Zagros Mountains, Iran. *Pet Geosci* 17(3):283–307
- Lønøy A (2006) Making sense of carbonate pore systems. *AAPG Bull* 90:1381–1405
- Mavko G, Jizba D (1991) Estimating grain-scale fluid effects on velocity dispersion in rocks. *Geophys* 56:1940–1949
- Mavko G, Mukerji T, Dvorkin J (1998) The rock physics handbook. Cambridge University Press
- Mavko G, Mukerji T, Dvorkin J (2009) The rock physics handbook, 2ed. Cambridge University Press
- Moshier SO (1989) Development of microporosity in amicroitic limestone reservoir, lower cretaceous, Middle East. *Sediment Geol* 63:217–240
- Nader FH, Swennen R (2004) Petroleum prospects of Lebanon: some remarks from sedimentological and diagenetic studies of Jurassic carbonates. *Mar Pet Geol* 21:427–441
- Neto IAL, Misságia RM, Ceia MA, Archilha NL, Hollis C (2015) Evaluation of carbonate pore system under texture control for prediction of microporosity aspect ratio and shear wave velocity. *Sediment Geol* 323:43–65. <https://doi.org/10.1016/j.sedgeo.2015.04.011>
- Nurmi R, Standen E (1997) Carbonates, the inside story. *Midd East Well Eval Rev* 18:28–41
- Pons A, David C, Fortin J, Stanchits S, Menéndez B, Mengus J-M (2011) X-ray imaging of water motion during capillary imbibition in porous rocks. Part 2: influence of compaction bands. *J Geophys Res* 116:B03205. <https://doi.org/10.1029/2010JB007973>
- Rafavich F, Kendall CHSC, Todd TP (1984) The relationship between acoustic properties and the petrographic character of carbonate rocks. *Geophys* 49:1622–1636
- Ravalec ML, Darot M, Reuschlé T, Guéguen Y (1996) Transport properties and microstructural characteristics of a thermally cracked mylonite. *PAGEOPH* 146:207–227
- Raymer DS, Hunt ER, Gardner JS (1980) An improved sonic transit time-to-porosity transform. Paper presented at the SPWLA 21st Annual Logging Symposium, 1–12, Soc. Prof. Well log analysts, Lafayette, La., 8–11 July
- Regnet JB, Robion P, David C, Fortin J, Brigaud B, Yven B (2015) Acoustic and reservoir properties of microporous carbonate rocks: implication of micrite particle size and morphology. *J Geophys Res Solid Earth* 120. <https://doi.org/10.1002/2014JB011313>

- Salah MK, Zhao D (2003) 3-D seismic structure of Kii peninsula in Southwest Japan: evidence for slab dehydration in the forearc. *Tectonophysics* 364:191–213. [https://doi.org/10.1016/S0040-1951\(03\)00059-3](https://doi.org/10.1016/S0040-1951(03)00059-3)
- Salah MK, Şahin Ş, Aydın U (2011) Seismic velocity and Poisson's ratio tomography of the crust beneath East Anatolia. *J Asia Earth Sci* 40: 746–761. <https://doi.org/10.1016/j.jseae.2010.10.021>
- Salah MK, El Ghandour MM, Abdel-Hameed AT (2016) Effect of diagenesis on the petrophysical properties of the Miocene rocks at the Qattara depression, North Western Desert, Egypt. *Arab J Geosci* 9: 329. <https://doi.org/10.1007/s12517-015-2275-8>
- Salah MK, Alqudah M, Abd El-Aal AK, Barnes C (2018) Effects of porosity and composition on seismic wave velocities and elastic moduli of lower cretaceous rocks, central Lebanon. *Acta Geophysica*. <https://doi.org/10.1007/s11600-018-0187-1>
- Sanjuan J, Alqudah M (2018) Charophyte flora from the Miocene of Zahle (Beeka Valley, Lebanon): biostratigraphic, palaeoenvironmental and palaeobiogeographical implications. *Geodiversitas* 40(10):195–209
- Schlumberger Ltd (2013) Oilfield Glossary, the Poisson's Ratio. Available at: http://www.glossary.oilfield.slb.com/en/terms/poissons_ratio.aspx (accessed 22.07.13)
- Sharland PR, Archer R, Casey DM, Davies RB, Hall SH, Heward AP, Horbury AD, Simmons MD (2001) Arabian plate sequence stratigraphy. *GeoArabia Spec Publ* 2, Gulf PetroLink, Bahrain, 371 p
- Siebold A, Walliser A, Nardin M, Oppliger M, Schultz J (1997) Capillary rise for thermodynamic characterization of solid particle surface. *J Colloid Interface Sci* 186:60–70. <https://doi.org/10.1006/jcis.1996.4640>
- Siegesmund S, Dürrast H (2014) Physical and mechanical properties of rocks. In: Stone and Architecture, by Siegesmund, S., Snethlage, R. (eds.), Springer-Verlag Berlin Heidelberg, DOI: https://doi.org/10.1007/978-3-642-45155-3_3
- Simmons G, Wang H (1971) Single crystal elastic constants and calculated aggregate properties. A handbook, MIT Press
- Soete J, Kleipool LM, Claes H, Hamaekers H, Kele S, Özkul M, Foubert A, Reijmer JGG, Swennen R (2015) Acoustic properties in travertines and their relation to porosity and pore types. *Mar Pet Geol* 59: 320–335. <https://doi.org/10.1016/j.marpetgeo.2014.09.004>
- Sun YF, Berteussen K, Vega S, Eberli GP, Baechle GT, Weger RJ, Massaferrero J L, Bracco Gartner GL, Wagner PD (2006) Effects of pore structure on 4D seismic signals in carbonate reservoirs. *SEG Tech Prog Expanded Abst* 3260–3264. <https://doi.org/10.1190/1.2370208>
- Vanorio T, Mavko G (2011) Laboratory measurements of the acoustic and transport properties of carbonate rocks and their link with the amount of microcrystalline matrix. *Geophys* 76:E105–E115. <https://doi.org/10.1190/1.3580632>
- Verwer K, Braaksma H, Kenter J (2008) Acoustic properties of carbonates: effects of rock texture and implications for fluid substitution. *Geophys* 73:B51–B65. <https://doi.org/10.1190/1.2831935>
- Walley CD (1997) The lithostratigraphy of Lebanon: a review. *Leb Sci Bull* 10:1
- Walsh JB, Brace WF (1984) The effect of pressure on porosity and the transport properties of rock. *J Geophys Res* 89:9425–9431
- Wang Z, Hirsche WK, Sedgwick G (1991) Seismic velocities in carbonate rocks. *Can Pet Tech* 30:112–122
- Weger RJ, Eberli GP, Baechle GT, Massaferrero JL, Sun Y (2009) Quantification of pore structure and its effect on sonic velocity and permeability in carbonates. *AAPG Bull* 93(10):1297–1317. <https://doi.org/10.1306/05270909001>
- Wilkens R, Simmons G, Caruso L (1984) The ratio V_p/V_s as a discriminant of composition for siliceous limestones. *Geophys* 49:1850–1860
- Wyllie MRJ, Gregory AR, Gardner LW (1956) Elastic wave velocities in heterogeneous and porous media. *Geophys* 21:41–70
- Wyllie MRJ, Gregory AR, Gardner GHF (1958) An experimental investigation of factors affecting elastic wave velocities in porous media. *Geophys* 23:459–493
- Xu S, Payne M, Exxonmobil (2009) Modeling elastic properties in carbonate rocks. *Lead Edge* 28:66–74
- Yu C, Ji S, Li Q (2016) Effects of porosity on seismic velocities, elastic moduli and Poisson's ratios of solid materials and rocks. *J Rock Mech Geotech Eng* 8:35–49. <https://doi.org/10.1016/j.jmge.2015.07.004>
- Zhang T, Dou Q, Sun Y (2012) Improving porosity-velocity relations using carbonate pore types. *SEG Las Vegas 2012 Ann Meet*, <https://doi.org/10.1190/segam2012-1214.1>
- Zhao D, Negishi H (1998) The 1995 Kobe earthquake: seismic image of the source zone and its implications for the rupture nucleation. *J Geophys Res* 103:9967–9986
- Zhao D, Kanamori H, Negishi H (1996) Tomography of the source area of the 1995 Kobe earthquake: evidence for fluids at the hypocenter? *Science* 274:1891–1894